Bimetal structures manufacturing with wire arc additive manufacturing (WAAM): review of microstructure, interface, and mechanical properties

Melike Korganci[1], Nurefşan Kuvvet[2], Yahya Bozkurt[3], Sezgin Ersoy[4]
[1, 2, 3]Marmara University, Technology Faculty, Metallurgy and Materials Engineering Department, Istanbul, Turkey
[4]Marmara University, Technology Faculty, Mechatronics Engineering Department, Istanbul, Turkey
[4]Corresponding author
E-mail: [1]*melike.korganci@marmara.edu.tr*, [2]*nurefsan.kuvvet@marmara.edu.tr*, [3]*ybozkurt@marmara.edu.tr*, [4]*sersoy@marmara.edu.tr*

Received 27 October 2025; accepted 21 February 2026; published online 9 July 2026
DOI https://doi.org/10.21595/jme.2026.25730

Abstract. Bimetallic structures are heterogeneous systems that combine the advantages of two different metallic materials, thereby providing tailored physical and mechanical properties for specific applications. In recent years, wire arc additive manufacturing has emerged as a promising technology for producing bimetallic structures, thanks to its high deposition rates and material efficiency. The use of wire arc additive manufacturing in the fabrication of bimetallic structures enables the production of different alloys within a single component, thereby paving the way for functionally graded and multi-material designs. The microstructures of bimetallic components produced using this method exhibit heterogeneities depending on the heat input, interlayer thermal stresses, intermetallic phase formation, and processing parameters. Mechanical properties, such as tensile strength, yield strength, and hardness, are directly dependent on the interfacial bonding conditions. At interfaces where brittle intermetallic phases form, a loss of ductility and an increased tendency to fracture are observed. A sufficient metallurgical bonding between two metallic materials results in acceptable mechanical performance in bimetallic structures built using wire arc additive manufacturing. Alloy compatibility, heat input control, and interface properties are critical for the successful application of bimetallic structures produced using this method. This review comprehensively evaluates the microstructural properties, mechanical behavior, and challenges of bimetal structures produced by wire arc additive manufacturing. The novelty of this review lies in its integrative analysis of interface-microstructural evolution and mechanical response, providing a unified perspective that has not been explicitly addressed in earlier studies. In addition, this study aims to provide a guiding framework for future research by presenting the relationship between the microstructure and mechanical properties of bimetallic structures fabricated using wire-arc additive manufacturing.

Keywords: wire arc additive manufacturing, bimetallic structure, interface, microstructure.

1. Introduction

ASTM International defines additive manufacturing (AM) as “a process of joining materials to make objects from 3D model data, usually layer upon layer, as opposed to subtractive manufacturing methodologies.” Unlike traditional subtractive techniques, AM builds components incrementally based on digital 3D data [1-3]. AM is considered one of the key components of Industry 4.0. Unlike conventional manufacturing methods, it operates on a fundamentally different principle that involves layer-by-layer deposition of material [4-6]. This method enables the production of complex geometries and large-scale metallic structures with reduced material consumption, fewer post-processing steps, and lower overall production costs, which has led to growing interest in AM [7-10]. Over the past three decades, the scope of AM technology has undergone a significant transformation. Initially, AM was primarily used for prototyping

applications aimed at design verification, shape, and fit evaluation; however, it is increasingly employed as a direct manufacturing method for end-use products [11, 12]. The geometric freedom and material flexibility offered by AM technologies provide new opportunities for product design [13-15]. The advantages of additive manufacturing include reductions in time, cost, material waste, and human intervention, thereby shortening the overall product development cycle [16-18]. Owing to its capability to fabricate complex and lightweight structures, AM has become a highly attractive manufacturing method in the aerospace industry [19-22].

Wire Arc Additive Manufacturing (WAAM) is an efficient additive manufacturing technique for producing medium- to large-scale, high-strength metal components [23]. It has been successfully applied in the aerospace industry for manufacturing structural parts such as wing spars and landing gear components, as well as in marine and offshore applications for producing ship propellers and critical offshore structure components [24,25]. Within aerospace applications, wall-type structures have been fabricated using the WAAM process, and the mechanical properties of these structures are comparable to those of conventionally cast or wrought products [26, 27]. In this method, based on data obtained from CAD models, welding wires are deposited layer by layer along a predetermined deposition path, enabling the production of various components with high dimensional accuracy [28, 29]. A schematic of the WAAM process is shown in Fig. 1. In this context, welding-based manufacturing technologies that utilize an electric arc as the heat source and a metal wire as the feedstock material have drawn considerable attention [30, 31]. The concept of fabricating entire components by depositing weld metal has been employed since the early 20th century [32]. In robotic WAAM structures, the macro- and microstructural characteristics of the fabricated parts vary significantly with the welding parameters. These parameters include variables such as the deposition rate, welding current, shielding gas type, wire feed speed, and heat input [33, 34]. These variables have a direct influence on the resulting mechanical and dimensional properties. Gas Metal Arc Welding (GMAW) is a welding process in which an electric arc is established between a consumable electrode and a workpiece [35, 36]. This method, which employs an electric arc as a heat source and continuously feeds filler wire into the molten pool to form the part, is essentially defined as a conventional wire-fed welding process [32, 37, 38]. Wire-fed methods eliminate many of the issues encountered in powder-based techniques [39, 40].

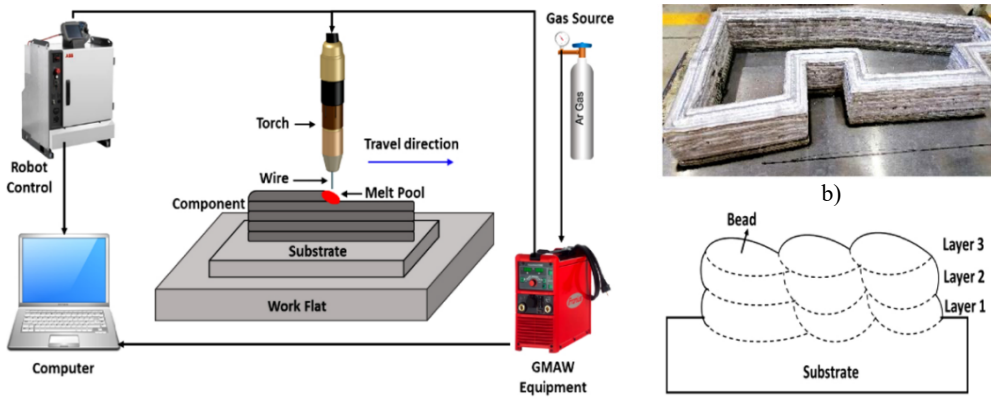

Fig. 1. a) Schematic of the WAAM system, b) photograph of a sample part, and c) detailed schematics of the sample cross sections [41]

This approach is implemented as the WAAM process. By utilizing robotic systems, WAAM allows the fabrication of complex geometries, thereby overcoming many of the limitations of traditional manufacturing methods [42]. One of the major advantages of the WAAM process is its relatively low capital investment, as WAAM equipment can be assembled from commercially

available, open-source components supplied by the welding industry [43, 44]. Due to its high deposition rate, relatively low production cost, and wide accessibility, WAAM has emerged as a prominent technology among metal additive manufacturing techniques [33]. It has become a promising approach for the fabrication of components made from various materials such as titanium, nickel-based superalloys, steel, and aluminium [8, 45]. Compared with other metal additive manufacturing processes, WAAM offers higher deposition rates, lower raw material costs, and improved dimensional accuracy [46-49]. However, due to the high heat input, issues related to residual stresses and surface quality can occur [41, 50]. The advantages and disadvantages of the WAAM process are listed in Table 1. According to the ASTM F2792-12a standard, WAAM is classified under the "Directed Energy Deposition" (DED) category [1]. Processes in this category are particularly advantageous for the cost-effective production of large, medium-complexity metal components. In addition, they provide significant raw material savings compared with conventional methods such as CNC machining and forging [51]. DED processes do not require specific molds, as in casting or forging, and therefore significantly reduce production costs and cycle times, particularly for low production volumes [52]. The use of wires in DED enables highly efficient material deposition [53].

Table 1. Advantages and disadvantages of WAAM [54]

Feature	Advantages	Drawbacks
Deposition rate	Enables high build rates suitable for large-scale component manufacturing	Not ideal for detailed or complex geometries
Material utilization	Efficient material usage with a low buy-to-fly ratio and minimal waste	Surface quality may require additional finishing operations
Heat input control	Provides improved heat management compared to powder-based AM methods	Repeated thermal cycles can lead to residual stress formation
Component size capability	Allows fabrication of large and robust structural components	Dimensional accuracy and resolution may be restricted
Cost-effectiveness	Offers a cost-efficient approach for manufacturing large metal parts	High equipment cost and operator expertise requirements
Multi-material fabrication	Demonstrated feasibility for producing bimetallic and functionally graded materials (FGMs)	Challenges exist in controlling the interfaces and achieving sound metallurgical bonds.

Over time, several terms have been used to describe WAAM, including Rapid Prototyping (RP), Shape Welding (SW), Shape Melting (SM), Solid Freeform Fabrication (SFF), Shape Metal Deposition (SMD), and 3D Welding [55-57]. The most commonly used processes in WAAM are TIG, MIG, and plasma arc-based approaches [58]. MIG-based WAAM exhibits significantly higher deposition rates than TIG and plasma-based methods [27, 30, 59]. As the wire is completely melted and fed into the molten pool, issues related to material accumulation are minimized [39]. However, in MIG-based WAAM, defects may occasionally occur due to the overflow or instability of the molten metal pool during the layer-by-layer deposition process. This issue can be mitigated by optimizing parameters such as the travel speed, wire feed rate, and torch-workpiece angle [10]. In conventional arc-based AM methods, spatter formation caused by high temperatures is frequently observed, which negatively affects the formability and overall shape accuracy of the produced part [60,61]. To eliminate this issue, to reduce the heat input, and stabilize the process, a variant of the GMAW method known as Cold Metal Transfer (CMT) was developed [8]. In arc-based manufacturing processes, the CMT technique effectively prevents problems such as excessive deformation and reduced forming precision [62, 63]. This system detects the moment when the wire contacts the molten pool and retracts it via a servo motor, thereby enabling a controlled and repeatable droplet transfer [64, 65]. The mechanism of the CMT technique is illustrated in Fig. 2.

In industrial applications requiring specialized functional performance, the additive manufacturing of bimetallic components has gained increasing importance due to the growing

demand for materials that can simultaneously provide conflicting properties such as high strength, low weight, corrosion resistance, and thermal stability [33, 54]. The demand for joining dissimilar metals has increased in industries such as power generation, petrochemicals, and the aerospace sector, to reduce material costs and enhance design flexibility [67]. By combining two different materials, bimetallic systems enable the production of composites with high mechanical strength, superior corrosion resistance, and good electrical conductivity [63, 68]. These properties are particularly critical in the automotive, energy, and aerospace sectors [69-71]. Welded joints of different metals in the production of power plant components are emerging, particularly to improve overall plant efficiency and prevent premature failure in critical welding areas [72]. Bimetallic composites fabricated using conventional manufacturing techniques have been reported to suffer from various drawbacks, such as interfacial cracking, the formation of brittle intermetallic phases, porosity, residual stresses, and pronounced microstructural heterogeneity [73-75]. Similarly, dissimilar welding processes involve inherent challenges, including the presence of unmixed zones, non-uniform elemental diffusion, and elevated residual stresses, which collectively degrade joint integrity and mechanical performance [76]. In conventional dissimilar welding, the weld interface often exhibits macro-segregation features, such as islands and peninsulas, along with pronounced elemental diffusion between the joined materials, resulting in compromised structural integrity [77]. Moreover, conventional manufacturing routes generally involve multi-step processes, complex equipment requirements, long production times, and high costs [78]. Today, bimetallic materials can be fabricated using modern additive manufacturing (AM) technologies [79-81]. In recent years, the WAAM process has emerged as a promising technology for the production of such structures owing to its high deposition rate, low cost, and efficient material utilization [54, 82, 83].

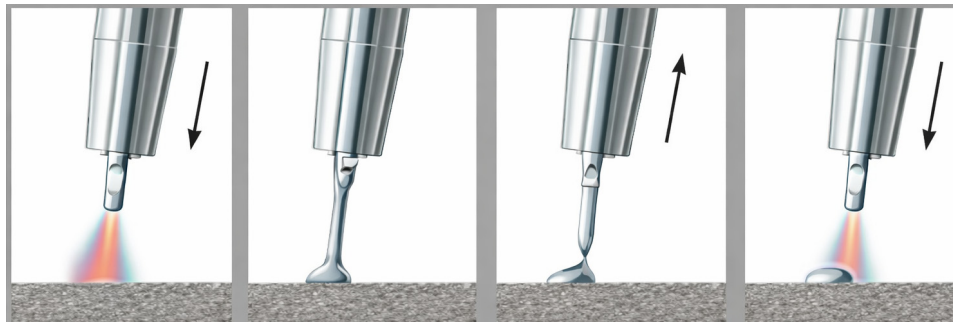

Fig. 2. One cycle of the wire retraction mechanism in the CMT technique [66]

Singh et al. [84] successfully fabricated, for the first time, bimetallic structures composed of NiTi (Nitinol) and stainless steel (SS 316L) alloys using the WAAM technique. In their study, the fabricated bimetallic wall exhibited a defect-free macrostructure and a typical layer-by-layer morphology characteristic of the WAAM process. Elemental analyses revealed a gradual transition in the distribution of Cr, Ti, and Fe across the interface; however, the formation of brittle intermetallic phases such as $TiCr_2$, FeNi, $TiNi_3$, and Ti_2Ni was also observed. The presence of these intermetallic phases increased the hardness while simultaneously reducing the ductility. Consequently, although a macroscopically sound structure was obtained, the mechanical behavior of the fabricated samples was brittle.

Gogulraj and Rajamurugan [85] successfully fabricated bimetallic overlapping structures of DSS-2507 and IN-625 alloys using the WAAM-CMT process. The produced structures demonstrated proper metallurgical bonding across the overlapping zone, as confirmed by comprehensive microstructural analyses. Microhardness measurements indicated that the thermal input influenced the grain size and phase distribution in both DSS-2507 and IN-625 regions, with the overlapping zone exhibiting intermediate hardness values. FESEM and EDX investigations revealed the effective intermixing of the two materials and the presence of chromium segregation

in the overlap. EBSD analysis provided detailed insights into the grain orientation, misorientation angles, and CSL boundaries, supporting the mechanical integrity of the bimetallic joint. This study highlights WAAM-CMT as an effective technique for producing dissimilar metal bimetallic structures with a controlled microstructure and promising mechanical performance.

Despite the demonstrated capability of Wire Arc Additive Manufacturing (WAAM) in producing medium- to large-scale metallic components, its application to bimetallic structures remains constrained by challenges such as unmet mechanical property requirements, high residual stresses, and the need for post-deposition treatments [32], as well as issues related to intermetallic phase formation, weldability, and thermophysical mismatches between dissimilar metals [86]. In this context, this review aims to comprehensively evaluate the potential of WAAM for the fabrication of bimetallic structures by examining the influence of process parameters, microstructural evolution, and mechanical performance based on current literature. Particular emphasis is placed on the effectiveness of advanced wire feeding techniques, such as WAAM-CMT, in achieving sound bimetallic bonding, with a focus on interfacial microstructural transformations and their impact on material properties. Accordingly, this review provides a systematic overview of recent developments, identifies the advantages and limitations of WAAM-based bimetal production, and offers an integrated perspective to guide future research and engineering applications in this emerging field.

2. Recent research progress in the GMAW-WAAM of bimetallic structures

Bimetallic structures are multi-material components designed to combine the advantageous properties of two metals. These properties include mechanical, thermophysical, and electrical characteristics, as well as enhanced corrosion and oxidation resistance [87, 88]. Various bimetallic studies have been conducted using the GMAW-WAAM process with different combinations, process parameters, and wire diameters. The most preferred materials for bimetal production with WAAM are stainless steel, nickel, low carbon steel, and copper alloys. Many studies have investigated the metallurgical and mechanical properties of bimetallic structures produced using WAAM. Ahsan Md. R. U. et al. [87] fabricated a bimetallic structure using 316L stainless steel and IN625 Inconel wires through the GMAW-WAAM (CMT) process. Microstructural examinations revealed that the 316L side of the layered structure consisted of ferrite dendrites within an austenitic matrix, whereas the IN625 side exhibited a completely austenitic microstructure (Fig. 3(a)). An increase in Laves phases was observed, particularly in the upper layers, due to the increase in Nb. These phases can be reduced using appropriate heat treatment methods. Ni, Nb, and Mo elements are dominant on the In625 side, while higher Fe contents are observed in the SS316L region (Fig. 3(b)). No intermetallic phase formation was observed at the interface between the two materials. Furthermore, continuous grain growth in the <001> direction of the FCC crystal structure was reported at the interface (Fig. 3(c-d)). This is a promising result for metallurgical bonds. Metallurgical bonding at the interface was achieved through thermomechanical equilibrium induced by thermal cycles and limited elemental diffusion. Consequently, epitaxial grain growth occurred, restricting segregation and the formation of brittle phases at the interface. Mechanical testing demonstrated high ductility with an ultimate tensile strength (UTS) of approximately 600 MPa and an elongation of 40 %. Fracture consistently occurred on the 316L side, further confirming the strong interfacial bonding between the two alloys. Sasikumar et al. [89] and Motwani et al. [90] also fabricated 316L-IN625 bimetallic structures using the WAAM process. These studies yielded microstructures and mechanical results similar to those obtained by Ahsan et al. [87]. Although the interface exhibited a distinct compositional gradient, no cracks, porosity, or intermetallic phase formation were observed. Moreover, mechanical testing revealed that fractures occurred on the 316L side in a ductile manner. These studies on the 316L-IN625 bimetallic structure support each other by revealing the microstructural continuity of the structure, the formation of the Laves phase, and its high mechanical properties.

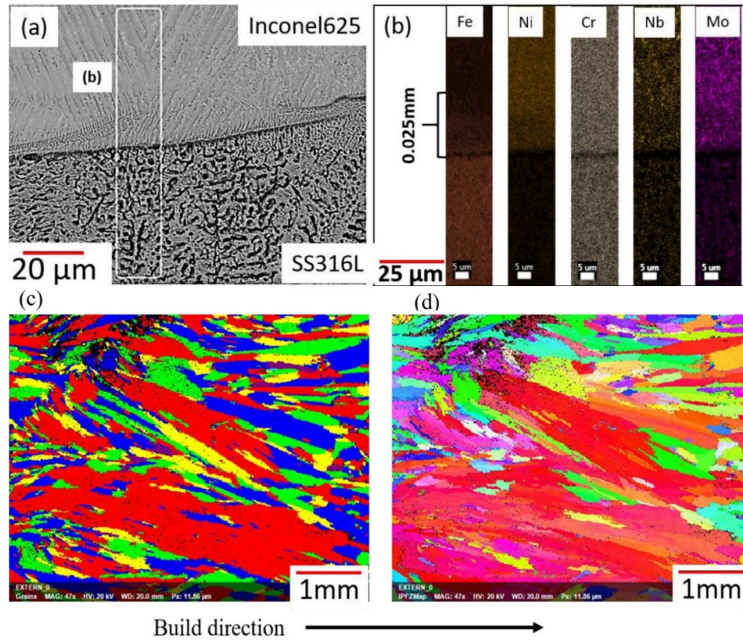

Fig. 3. Analysis results at the interface: a) SEM micrograph with the location for elemental mapping, b) elemental mapping data, c) EBSD grain map, and d) EBSD IPF [87]

In another study involving 316L and IN625, Zhang et al. [91] fabricated a 316L-IN625 bimetallic structure using the GMAW-WAAM (CMT) process. The study compared two different deposition strategies: first 316L, then IN625 (316L-IN625) and first IN625, then 316L (IN625-316L). Microstructural analyses revealed that while the deposition strategy did not alter the overall microstructure, it significantly influenced the δ-ferrite morphology and the amount of Laves phase. In the 316L section, the δ-ferrite structure transformed from a lamellar form to a skeletal form as the number of layers increased. No defects were observed at the interface of the 316L-IN625 structure. However, when 316L was deposited onto IN625, remelting of IN625 occurred, leading to enhanced Fe-Ni diffusion and the formation of the Laves phase due to Nb-Mo enrichment. Consequently, interfacial cracks were formed as a result of increased thermal cycling and associated residual stresses. Mechanical testing revealed that the 316L-IN625 configuration exhibited a UTS of 444 MPa with an elongation of 38.6 %, and fractures occurred on the 316L side. In contrast, the IN625-316L configuration achieved a UTS of 406 MPa and an elongation of 23.6 %, with fracture initiation at the interface. This study clearly demonstrates the critical influence of deposition strategy on the structural integrity and mechanical performance of WAAM-fabricated bimetallic components. When studies conducted on stainless steel and Inconel 625 are evaluated, it is observed that the interfacial behavior is directly dependent on thermal cycles, elemental diffusion, and the deposition strategy. Ahsan et al. [87], Sasikumar et al. [89], and Motwani et al. [90] reported interfaces devoid of cracks and intermetallic phases in their studies. In contrast, Zhang et al. [91] observed in their study that the occurrence of interfacial cracks varied depending on the deposition strategy. These cracks are attributed to an increase in Laves phase formation resulting from the remelting of IN625, depending on the deposition strategy. These contrasting findings indicate that the interfacial characteristics of WAAM-fabricated 316L-IN625 bimetallics depend not only on the material combination but also on the deposition strategy.

Raut L. P. and Taiwade R. V. [92] produced a bimetallic structure using GMAW-WAAM(CMT) technology with LCS (ER70S-G) and 316LSi wires. In microstructural examinations, δ-ferrite was observed within the austenitic matrix on the SS316LSi side, while

polygonal ferrite was observed on the LCS side. No defects were observed at the interface. However, the diffusion of Cr from 316LSi to the LCS side was observed. Due to the solid solution hardening of Cr, the hardness of the interface increased by 22 %. Marefat F. et al. [93] produced a bimetal structure using 316L and LCS wires with GMAW-WAAM (CMT). In the study, the LCS was first deposited, then the WAAMed LCS wall was rotated 90°, and 316L was deposited onto the lateral surface of the LCS wall. The results demonstrated that when the second wire was deposited perpendicular to the deposition direction of the first wire, the interfacial shear strength increased by approximately 10 %. This improvement was attributed to the formation of interlocking regions at the interface (Fig. 4). This region was formed as a result of molten LCS and 316L flowing into each other without complete dissolution, thereby enabling more effective shear load transfer. Microstructural analyses revealed a martensitic transformation at the interface associated with carbon diffusion (Fig. 5). As a result of thermodynamic and diffusion mechanisms, the interfacial hardness increased to 463 HV.

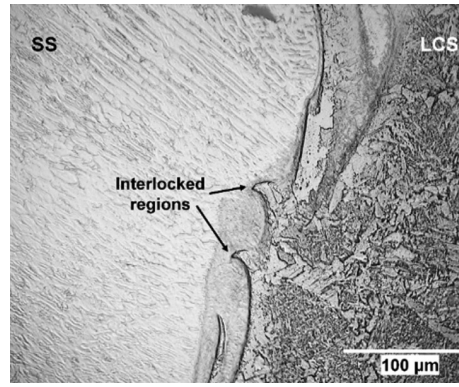

Fig. 4. Interlocking at the interface of 316L/LCS WAAM wall [93]

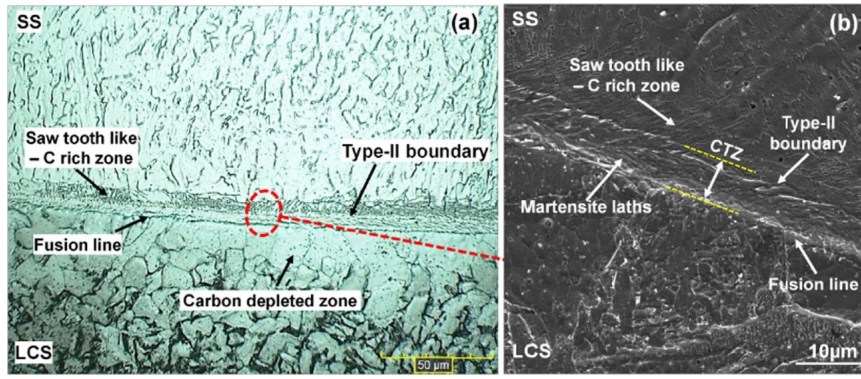

Fig. 5. Microstructural characteristics of the LCS-SS316L bimetallic interface [93]

Ahsan Md. R. U. et al. [94] fabricated a bimetallic structure using LCS (ER70S6) and 316L stainless steel wires by the GMAW-WAAM (CMT) process and investigated the effects of post-heat treatment on its microstructural and mechanical properties. It was determined that the 950 °C, 1-hour condition was the optimum condition for the heat treatment applied to the LCS-316L bimetallic structure. Under these conditions, the UTS, yield strength (YS), and elongation increased by approximately 35 %, 25 %, and 250 %, respectively. These results demonstrate that post-heat treatment of WAAM-fabricated structures effectively improves both strength and ductility by stabilizing intermetallic phase formation. Furthermore, the fracture that occurred on the LCS side before heat treatment shifted to the 316L side after heat treatment. This also indicates that heat treatment strengthens the bond strength at the interface. Microstructural

analyses revealed a ferrite-to-bainite transformation in the LCS region, while the 316L side exhibited a reduction in the δ-ferrite content. The results demonstrate the significant effect of heat treatment applied to bimetals produced using WAAM on microstructure and mechanical properties. Ayan Y. and Kahraman N. [95] produced a bimetallic structure using the WAAM method with ER70S-6 LCS and 308LSi wire. In this study, a bimetallic structure was fabricated by alternating the wire material in each layer. Microstructural examinations revealed δ-ferrite within the austenitic matrix on the 308LSi side and martensitic and bainitic phases in the LCS section (Fig. 6).

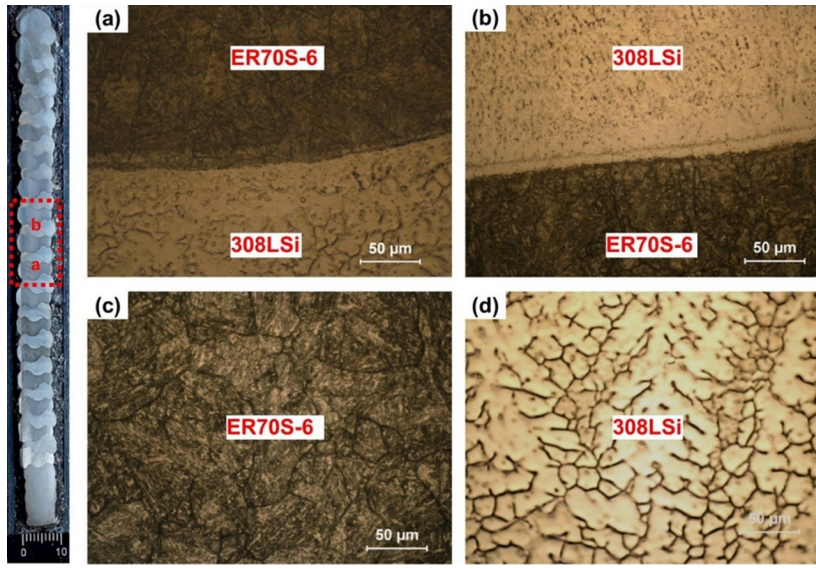

Fig. 6. Microstructure of the bimetallic structure: a) 308LSi-ER70S-6 interface, b) ER70S-6-308LSi interface, c) ER70S-6 side near the interface, and d) 308LSi side near the interface [95]

The high Cr and Ni contents in 308LSi are known to promote martensite formation. In the ferrite-dominated ER70S-6 matrix, these elements are unable to stabilize austenite, resulting in the formation of martensite. No intermetallic phases were detected at the interlayer interfaces; however, a high density of martensitic structures was observed. Martensite development at the fusion boundary occurs as a result of carbon diffusion into the Cr-enriched region [96]. Mechanical testing revealed a tensile strength of 709 MPa and 31 % elongation, indicating that diffusion-controlled phase transformations enhance interfacial bonding. The occurrence of fractures on the 308LSi side also proves the strength of the interface bond. Chen Y. et al. [34] produced a bimetallic structure using GMAW-WAAM by changing the wire in each layer using LCS (ER70S-6) and 304 wires. Microstructural examinations of the produced bimetallic structure revealed that the austenitic matrix in the 304 layer transformed into martensite, whereas the ferrite grains in the LCS layer were refined. These transformations were attributed to the presence of a diffusion zone approximately 30 µm thick at the interfacial region. EDS analysis revealed the diffusion of Fe-Cr-Ni elements across the layers and their transition without the formation of intermetallic phases (Fig. 7). As a result of the microstructural changes, mechanical testing yielded a tensile strength of 999.8 MPa and an elongation of 28.2 %. These values are nearly twice the tensile and elongation data of both LCS and 304 materials. When WAAM-fabricated LCS-stainless steel bimetallic structures are examined, the interfacial characteristics are controlled by elemental diffusion and the associated phase transformations. Specifically, the diffusion of Cr and Ni elements enhances solid solution strengthening, while the diffusion of C increases interfacial hardness due to martensitic transformation. Furthermore, it has been reported that process parameters such as the deposition strategy, build direction, and heat treatment are

determinative for the mechanical performance of the interface.

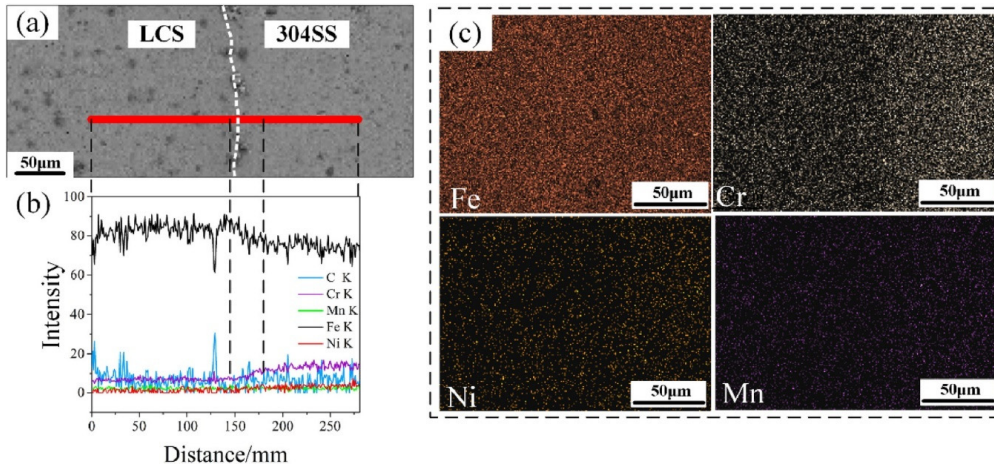

Fig. 7. a) SEM image of the LCS/304 SS interface with the marked location for EDS line scan and b) EDS line scan results, c) elemental mapping across the interface [34]

Ainapurapu S. B. et al. [97] fabricated a bimetallic structure using a hot-forged 304L substrate and 308L stainless steel wire using the GMAW-WAAM (CMT) process. In this study, two different metal transfer modes, pulsed and spray, were utilized in the WAAM-based fabrication of bimetallic structures. Microstructural analyses revealed epitaxial grain growth at the interface for both modes. Spray-mode deposition formed columnar and coarse δ-ferrite grains due to the continuous heat input, whereas pulsed-mode deposition, with an increased nucleation rate induced by rapid cooling, yielded finer epitaxial grains. The thermomechanical differences between the two modes led to an increase in microhardness to 247 HV and an enhancement in tensile strength in the pulsed mode. This study shows that thermomechanical mechanisms related to the metal transfer mode determine the microstructure and mechanical properties of WAAM-fabricated bimetallic structures. Wang X. et al. [98] fabricated bimetallic structures using the GMAW-WAAM (CMT) process with two different deposition strategies: 316L/430 and 430/316L. Microstructural examinations revealed that different heat inputs lead to grain growth, carbide precipitation, and martensitic formation in the ferritic regions. In the austenitic 316 L regions, the austenite + δ-ferrite structure was maintained. For the 430 materials, the microstructural evolution with increasing heat input proceeded as $F \rightarrow F + (Cr, Fe)_{23}C_6 \rightarrow F + M$. Thermodynamically induced phase transformations, especially at grain boundaries, led to martensite formation and consequently increased high-temperature brittleness. At the interface, the diffusion of Ni from the 316L side into the 430 side induced the formation of martensite and acicular ferrite. Consequently, the highest hardness value (337 HV) was measured near the interface on the 430 side. Mechanical testing showed that all specimens exhibited brittle fracture on the ferritic 430 side. Furthermore, the deposition strategy was found to significantly influence tensile strength, with the 430/316L strategy providing a higher ultimate tensile strength (265.8 MPa) compared to the 316L/430 strategy. Tanwar R. S. and Jhavar S. [99] produced a bimetallic structure using 316L and 309 wires with GMAW-WAAM. In this study, three layers were formed in 316L-309-316L. Microstructural investigations revealed that Cr and Ni diffusion occurred at the interface as a result of repeated melting-solidification effects. The high Cr content of the 309 steel increased the Creq/Nieq ratio at the interface and promoted solidification in the FA (ferrite–austenite) mode. Consequently, hot cracking at the interface was suppressed. Tribological testing showed that the coefficient of friction (CoF) of the bimetallic structure (0.42-0.58) was lower than that of 316L and 309 materials. This improvement was attributed to the increased surface hardness resulting from a higher ferrite phase fraction. After wear, Fe_2O_3,

Fe_3O_4, and CrO_2 oxide phases, as well as deformation-induced α-martensite formation, were observed on the surfaces. These oxide layers are considered to enhance surface stability during wear, thereby improving frictional characteristics. These results indicate that the 316L-309 combination is suitable for tribological components (pumps, valves, etc.) operating at high temperatures. When studies on stainless steel-based bimetallic materials produced by WAAM are considered together, it has been observed that the interfacial microstructure and mechanical behavior are related to heat input, deposition strategy, and metal transfer mode. Differences among metal transfer modes determine grain size and hardness distribution by altering nucleation rates and grain growth mechanisms. In different deposition strategies, phase transformations such as martensite formation and carbide precipitation occur. Furthermore, the diffusion of Cr and Ni at the interface, along with the increase in the Creq/Nieq ratio, promotes solidification in the FA mode, thereby preventing hot cracking. These findings indicate that interfacial integrity and mechanical performance can be optimized through appropriate process parameters.

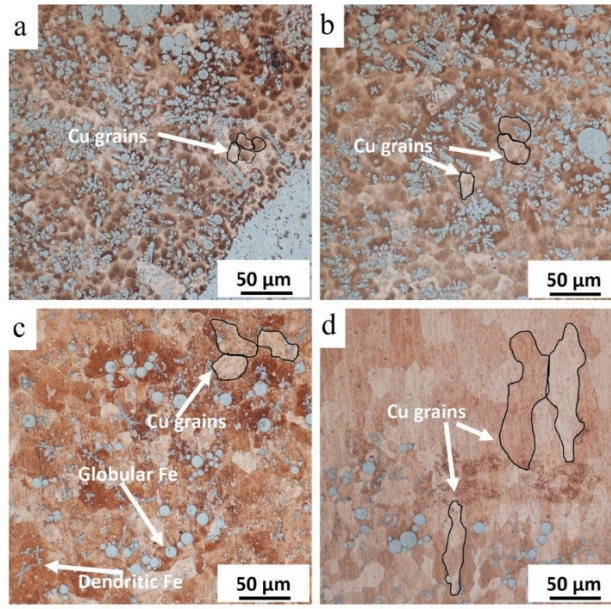

Fig. 8. The micrographs of 316L/Cu bimetallic structure at a) interface of 316L and Cu; b) center of 1st Cu layer; c) center of 2nd Cu layer; d) third Cu layer [101]

Kaur H. et al. [100] produced a bimetallic structure using CMT-WAAM with super duplex stainless steel (SDSS) and Inconel 625. The produced bimetallic structure was then subjected to an aging treatment at 800 °C for 2 hours. It was observed that the Cr, Ni, and Fe elements decreased, and C was enriched in the dendrite regions of SDSS and Inconel 625. This was relatively higher in the aged structure. Aging treatment resulted in the formation of NbC, γ'' (Ni_3Nb), and Laves phases (Ni_2Ti, Cr_2Ti). In corrosion tests, the structure exhibited the highest pitting potential of 840.8 mV before aging, while this value decreased to 372.1 mV after aging. This loss of pitting resistance was associated with the formation of NbC and γ'' (Ni_3Nb) in the interfacial region. However, the overall corrosion rate decreased to 1.84×10^{-7} mpy. However, the overall corrosion rate decreased to 1.84×10^{-7} mpy. In conclusion, the SDSS/IN625 bimetal combination can improve corrosion performance, but thermal aging conditions need to be optimized. Tomar B. and Shiva S. [101] investigated a bimetallic structure produced using GMAW-WAAM (CMT) with 316L and pure copper (Cu) wires. Microstructural examinations revealed that the Fe phase on the Cu matrix solidified in a globular and dendritic morphology (Fig. 8(a-b)). This result is associated with the solidification of Fe as an Fe-rich discrete phase

within the Cu matrix due to the limited mutual solid solubility in the Fe-Cu system and the high cooling rates. Furthermore, a transition zone approximately 6 mm thick was observed, where Fe precipitated in a globular dendritic form within the Cu matrix (Fig. 8(c-d)). The formation of this transition region is considered to result from the inability to feed both wires simultaneously and from repeated melting-solidification cycles. Additionally, no intermetallic phases or defects were reported. This indicates that the formation of undesired phases in the Fe-Cu system can be limited using WAAM. The mechanical testing showed a UTS of 641 MPa in the horizontal direction and 427 MPa in the vertical direction, with an elongation of approximately 20 %. The mechanical performance of the bimetallic structure was found to be superior to that of pure Cu, but lower than that of 316L. Munusamy S. and Jerald J. [102] investigated a bimetallic structure fabricated by the GMAW-WAAM process using Grade 91 steel and Monel 400 wires. Microstructural examinations revealed that Grade 91 steel contained lath martensite and $M_{23}C_6$-type carbide precipitates, which increased its strength, while Monel 400 retained its ductility due to its homogeneous FCC structure (Fig. 9).

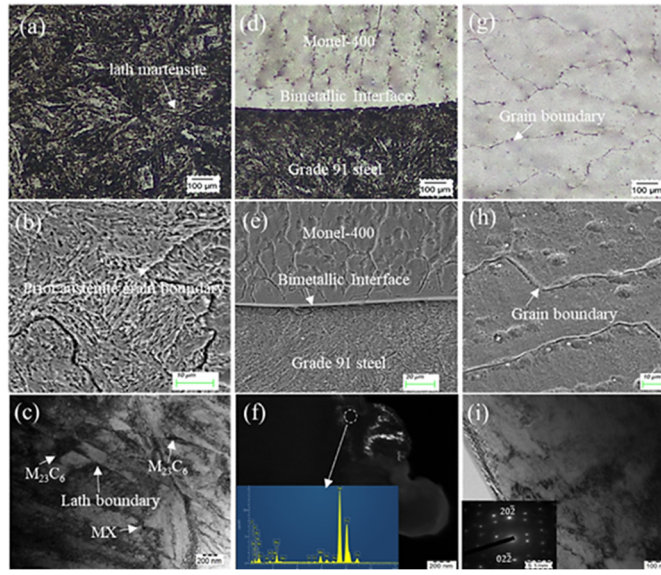

Fig. 9. Microstructure analysis of WAAM samples using OM, SEM, and TEM: a)-c) WAAMed wall grade 91 steel, d)-e) bimetallic interface, f) TEM/EDS analysis at the interface, g)-i) WAAMed wall Monel-400 [102]

SEM-EDS analyses reported the presence of Fe, Ni, Cr, and Cu elements in the interfacial region. The combination of these elements provides a balance between mechanical and corrosion properties. Ductile fracture was observed to be dominant in all samples. In addition, oxide phases such as Fe_2O_3, NiO, and CuO were observed on the surface. These phases contribute to hardness and corrosion resistance. Han S. et al. [103] produced a bimetallic structure using ER80S-G and MF6-55GP wires with GMAW-WAAM (CMT). Microstructural analyses revealed the presence of ferrite and pearlite phases in the ER80S-G layers, while the MF6-55GP layers exhibited martensite, retained austenite, and carbide precipitates. These findings indicate a pronounced difference in phase and hardness between the two materials. However, no pores or cracks were observed in the interfacial region. Thus, the low heat input of the CMT-WAAM process enabled the bonding of two dissimilar materials through a transition region. Mechanical testing showed that the bimetallic structure exhibited a UTS of 447.79±24.32 MPa, which was comparable to that of ER80S-G but lower than that of MF6-55GP. This reduction in strength was attributed to the accumulation of residual stress and microstructural discontinuities at the interface.

Meng et al. [104] investigated a bimetallic material produced using 316L stainless steel and

S214 bronze wires by the GMAW-WAAM (CMT) process. Different heat inputs and deposition strategies (316L/S214 and S214/316L) were used for the bimetal production. Microstructural analyses revealed that in the 316L layers, fine-grained austenite and lath ferrite formed under low heat input conditions, whereas a skeletal ferrite structure developed at higher heat inputs. In the S214 bronze layers, a transformation from an α-Cu + γ + Fe-rich phase to an α-Cu + Fe-rich phase + K phase was observed. This transformation can be attributed to the increased diffusion caused by the higher heat input. In the interface region, Fe-based solid solutions and intermetallic phases such as $AlCrFe_2$, $AlNi_3$, and Al_4Cu_9 were detected. It has been reported that although hardness increased due to these phases, the tendency for brittleness also increased. At low heat input, a wider transition region exhibiting a honeycomb morphology formed due to differences in diffusion behavior between Cu and Fe and the presence of large thermal gradients. With increasing heat input, Marangoni convection was enhanced, resulting in more homogeneous mixing within the interfacial region. Tensile tests revealed that the fracture occurred on the S214 bronze side of the bimetallic structure. The UTS varied with deposition strategy, reaching 500 MPa for S214/316L and 350 MPa for 316L/S214. Hasani N. et al. [105] produced a bimetallic structure using GMAW-WAAM (CMT) with Inconel 718 wire and S275 substrate material. The bimetallic structure was examined under three conditions: as-built (AB), solution-treated (ST), and solution-treated + aged (STA). In the AB condition, pronounced microsegregation (primarily of Nb) and the formation of Laves phases were reported due to rapid solidification and limited elemental diffusion (Fig. 10(a)). The ST treatment at 1080 °C was found to partially dissolve these phases, but was insufficient for complete dissolution (Figure 10(b)). Following solution treatment (ST), the flattening of grain boundaries was attributed to the partial dissolution of Laves phases and carbides. At higher solution treatment temperatures, grain coarsening occurred, which facilitated dislocation motion and consequently led to a degradation in mechanical properties.

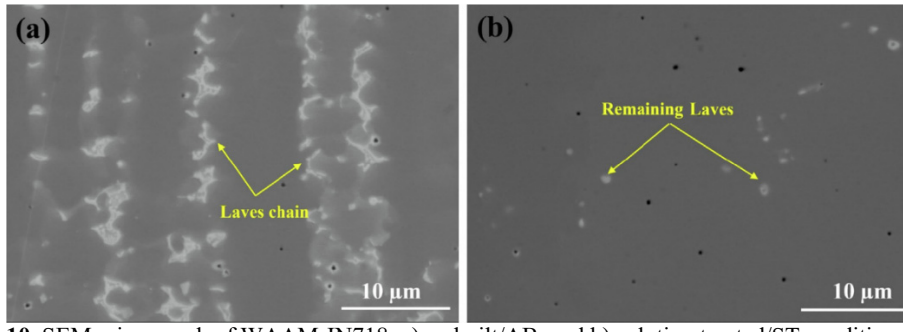

Fig. 10. SEM micrograph of WAAM-IN718: a) as-built/AB, and b) solution treated/ST conditions [105]

Spalek N. et al. [106] produced a bimetallic structure using GMAW-WAAM with high-strength X90 steel and high-ductility SG2 steel. EDX analysis revealed diffusion of Ni and Cr between the two steels. This diffusion resulted in a balance in hardness values, forming a similar microhardness profile for both materials in the range of approximately 185-195 HV. The absence of sharp hardness gradients indicates that no interfacial discontinuities were formed and that diffusion occurred in a controlled manner. In tensile tests, the bimetallic structure exhibited a UTS of 600 MPa and an elongation of 23 %. Based on these results, a balanced value emerged between SG2 and X90. Manohar G. et al. [107] investigated the use of a CuNi (70/30) interlayer in a bimetallic structure to be produced using WAAM with 304L and AA2319 aluminum. Microstructural analyses revealed that the CuNi interlayer acted as a diffusion barrier between the 304L and AA2319 layers. This barrier significantly reduced the formation of brittle intermetallic compounds, such as Fe_2Al_5 and $FeAl_3$, which typically form at the Al-Fe interface. Despite the increase in hardness due to the uniform diffusion of Fe, Ni, and Cu at the interface, no brittle phases were formed. However, intermetallic phases, such as AlCu and $AlCu_4Ni$, at the interface caused high local hardness but negatively affected ductility. These results demonstrate that the

CuNi interlayer strengthens the metallurgical bond in the WAAM-fabricated Al-steel bimetal by suppressing intermetallic formation; however, the intermetallic phases formed at the CuNi-Al interface continue to influence the mechanical behavior. Jadhav S. et al. [108] investigated the bimetallic structure produced using different heat inputs from Ti6Al4V and NbZr1 wires with the GMAW-WAAM method. Microstructural analysis revealed the absence of cracks, pores, or intermetallic compounds at the interface. Island and dendritic regions containing the (βTi, Nb) and ($\alpha + \beta$Ti, Nb) solid solutions were observed at the interface (Fig. 11). The formation of island-like regions is attributed to the difference in melting temperatures between the Ti6Al4V and NbZr1 alloys, as well as to the flow behavior within the molten pool. EDS analyses showed that Nb diffusion toward the Ti6Al4V side increased with increasing heat input. The enhanced Nb diffusion did not lead to the formation of intermetallic phases at the interface but instead promoted solid-solution formation. Microhardness measurements showed that the hardness at the interface decreased to 99.9-339 HV. Hardness differences at the interface are due to microstructural heterogeneities and changes in local composition. In tensile results, the highest UTS was 567 MPa at the 180A parameter (lowest heat input). Fractures occurred on the NbZr1 side of the specimens. This indicates that the bond at the interface is strong. Kesarwani S. et al. [109] produced a bimetallic structure using ER5356 (Al-Mg) and ER4043 (Al-Si) aluminum wires with GMAW-WAAM (CMT). The study was conducted under different deposition directions (unidirectional/bidirectional) and current combinations. The results showed that the bidirectional deposition strategy significantly improved microstructural integrity. In bidirectionally fabricated specimens, a more uniform heat distribution was achieved, resulting in equiaxed and fine-grained microstructures. In the unidirectional deposition strategy, pronounced heat accumulation detrimentally affected the solidification dynamics, leading to the formation of discontinuous dendritic structures and pronounced porosity. Furthermore, it has been shown that strength-enhancing intermetallic phases, such as Mg_2Si, $Al_{12}Mg_{17}$, and AlMg, are concentrated in this region (Fig. 12). This indicates that the thermal cycles varying with the deposition strategy directly influence elemental diffusion and phase formation. In mechanical tests, the bidirectional wall exhibited the best performance, with a UTS of 205 MPa and an elongation of 18.9 %. In unidirectional samples, strength and ductility decreased due to directional heat accumulation. Fractures occurred on the ER4043 side during the tensile tests. This indicates that the bimetallic interface has better strength than ER4043. When WAAM bimetal studies with different alloy combinations are examined, heat input, metal transfer mode, deposition strategy, and heat treatments directly influence the interfacial microstructure by determining the thermal cycles and phase transformations associated with element diffusion. At low heat inputs, epitaxial grain growth and solid solution formation are more dominant, whereas at high heat inputs, intermetallic phases, Laves phases, and martensitic transformations occur. In mechanical tests, the fact that fracture does not occur at the interface in many studies indicates the formation of a strong metallurgical bond through WAAM. These findings reveal that the performance of bimetallic structures produced by WAAM depends more on process parameters than on alloy combinations.

Recent studies on bimetallic structures produced using GMAW-WAAM have highlighted both the significant potential and inherent challenges of this additive manufacturing technique. WAAM allows the combination of different metals and alloys within a single component, enabling region-specific optimization of mechanical and corrosion-resistant properties. However, challenges such as interfacial intermetallic formation, residual stresses, and porosity remain critical issues, affecting the mechanical integrity and long-term performance of WAAM-produced bimetallic components. Several studies have proposed strategies to mitigate these challenges, including careful material selection, interlayer design, heat input control, and post-processing treatments, which can enhance the structural reliability of WAAM bimetal components. Overall, the literature indicates that WAAM holds great potential for industrial bimetallic manufacturing, but further research is needed to fully understand interfacial phenomena and to optimize processing conditions for reliable performance.

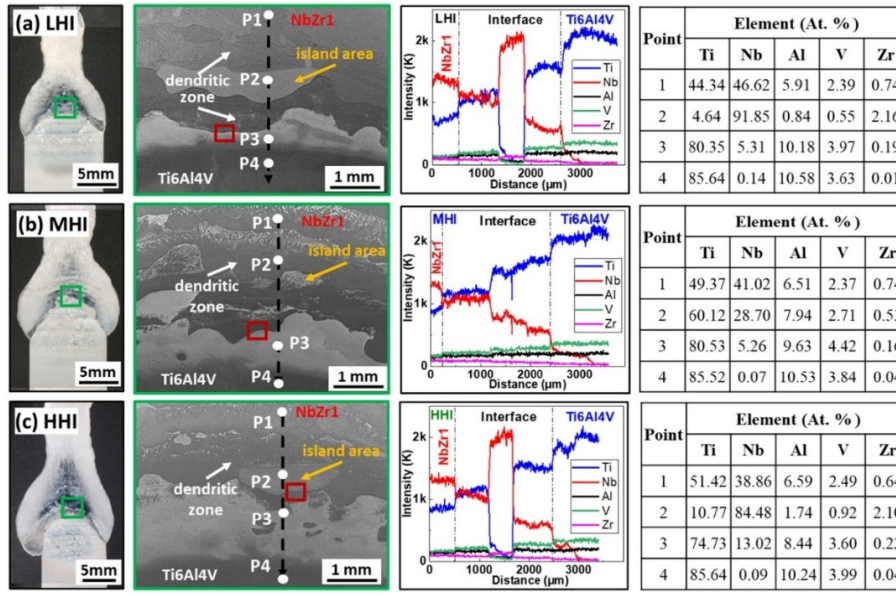

Point	Element (At. %)				
	Ti	Nb	Al	V	Zr
1	44.34	46.62	5.91	2.39	0.74
2	4.64	91.85	0.84	0.55	2.16
3	80.35	5.31	10.18	3.97	0.19
4	85.64	0.14	10.58	3.63	0.01

Point	Element (At. %)				
	Ti	Nb	Al	V	Zr
1	49.37	41.02	6.51	2.37	0.74
2	60.12	28.70	7.94	2.71	0.53
3	80.53	5.26	9.63	4.42	0.16
4	85.52	0.07	10.53	3.84	0.04

Point	Element (At. %)				
	Ti	Nb	Al	V	Zr
1	51.42	38.86	6.59	2.49	0.64
2	10.77	84.48	1.74	0.92	2.10
3	74.73	13.02	8.44	3.60	0.22
4	85.64	0.09	10.24	3.99	0.04

Fig. 11. EDS line and point scan results at the interface for the a) Low heat input (LHI), b) Medium heat input (MHI), and c) High heat input (HHI) conditions [108]

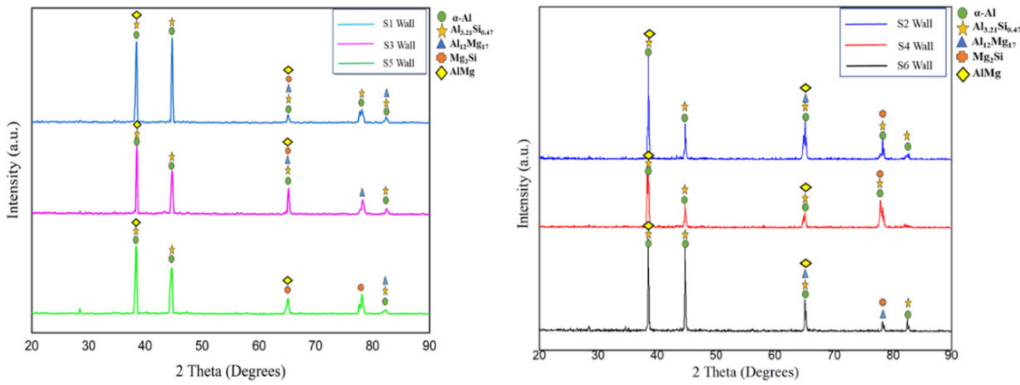

Fig. 12. XRD analysis at the interface layer of the bimetallic wall: a) bidirectional walls, b) unidirectional walls [109]

A comprehensive overview of studies on bimetallic structures fabricated by WAAM, including both GMAW-WAAM and its CMT variant, is presented in Table 2. The table covers numerous studies conducted on various material systems, such as steel, Inconel, titanium, aluminum, copper, and nickel-based alloys. For each system, the main process parameters, microstructural characteristics, and mechanical performance values are systematically presented, enabling a comprehensive comparison between different studies.

Table 2. Summary of studies on bimetallic structures fabricated using GMAW-WAAM

	Material combination	AM process	Process parameters	Findings	Ref.
Stainless steel	SS316L/IN625	GMAW-WAAM (CMT)	Wire diameter: 1.2 mm, Current: 200A (SS316L), 148A (IN625); Voltage: 13.1V (SS316L), 14.5V (IN625); WFS: 6.5 m/min; WS: 600 mm/min	No intermetallic phase formation was observed at the interface between the two materials. 600 MPa UTS, 40 % el.	[87]

	SS316L/IN625	GMAW-WAAM	Wire diameter: 1.2 mm, Current: 138A (SS316L), 132A (IN625); Voltage: 16.2V (SS316L), 15.3V (IN625); WFS: 3.8 m/min (SS316L), 3.68 m/min (IN625); WS: 400 mm/min	Columnar and coaxial dendrites were observed on the SS 316L side, and continuous grain growth was noted at the interface. Hardness: 198-214 HV, YS: 448 ± 12 - 531 ± 14 MPa, UTS: 804 ± 21 - 845 ± 20 MPa, % el.: %25 ± 2 -%19 ± 1	[89]
	SS316L/IN625	GMAW-WAAM (CMT)	Wire diameter: 1.2 mm, Current: 150A (SS316L), 120A (IN625); Voltage: 12.8V; WFS: 5.5 m/min (SS316L), 4.2 m/min (IN625); WS: 6 mm/sec.	Nb + Mo segregation has been detected in the dendritic regions of the IN625 microstructure. Hardness:160-190 HV (316L Si), 220-245 HV (IN625); UTS: 507-660 MPa, %El.: 55.9-49.3	[90]
	SS316L/IN625	GMAW-WAAM (CMT)	Wire diameter: 1.2 mm, Current: 85-160 A; Voltage: 16.4-20.0 V; WFS: 2.9-5.7 m/min; WS: 200 mm/min	No defects were observed on the interface of the 316L-IN625 structure. However, two interface cracks formed in the IN625-316L structure. UTS: 406.55-444.45 MPa, %el: 23-38	[91]
	SDSS/IN625	GMAW-WAAM (CMT)	Wire diameter: 1.2 mm, Current: 225A; Voltage: 19.4V; WFS: 9.5 m/min; WS: 25 cm/min	After the aging process, NbC, σ-phase, laves (Ni_2Ti, Cr_2Ti), and Ni_3Nb precipitates formed.	[100]
	SS321/IN625	GMAW-WAAM	Current: 160A (ER5356), Voltage: 16.8 V (ER5356); WFS: 2.83 kg/h (SS321), 2.99 kg/h (IN625); WS: 30 cm/min	No cracks or similar defects were observed. UTS: 628 ± 8, YS: 298 ± 7, %el.: 29.67 ± 1.5	[110]
	YS308L/Ni6082	GMAW-WAAM	Wire diameter: 1.2 mm, Current: 140A; Voltage: 20.6 V (YS308L), 24.2 V (Ni6082); WFS: 200 mm/min	The mechanical properties of the bimetal were comparable to those of a cast material.	[111]
Aluminum/ Aluminum	ER5356/ER4043	GMAW-WAAM (CMT)	Wire diameter: 1.2 mm, Current: 115-125A (ER5356), 90-100A (ER4043); Voltage: 14.6-15.1V (ER5356), 13.5-14.0V (ER4043); WFS: 7.8 -8.3 m/min (ER5356), 6-6.6 m/min (ER4043); WS: 6 mm/sec	Porosity defects were observed throughout all six deposited walls. UTS: 205,73 MPa, %el.:18.94	[109]
	AA5083/AA6061	GMAW-WAAM (CMT)	Current: 177A, Voltage: 15.3 V; WFS: 8 m/min (SS321); WS: 6 mm/s	Al(Fe, Mn)Si and Al(Fe, Mn, Cr, Ti)Si intermetallics were formed between the layers	[112]
Low carbon steel / Stainless steel	LCS-316L	GMAW-WAAM (CMT)	Wire diameter: 1.2 mm, Voltage: 12.8-15V; WFS: 4.5-7.5 m/min; WS: 200-400 mm/min	Despite its heterogeneity, the bimetallic interface is structurally sound and defect-free. Hardness: 463 HV	[93]
	LCS (ER70S-G)/316L	GMAW-WAAM (CMT)	Wire diameter: 1.2 mm, Current: 110A (LCS), 90A (316L); Voltage: 12.5V (LCS), 11.9V (316L); WFS: 2.9 m/min (LCS), 2.3 m/min (316L); WS: 114 mm/min (LCS), 96 mm/min (316L)	No intermetallic phase was observed at the interface. YS: 306,54 MPa, UTS: 493,11 MPa, %el.: 22,70	[92]

	LCS (ER70S6)/316L	GMAW-WAAM (CMT)	Wire diameter: 1.2 mm, Current: 15.9A (LCS), 13.1A (316L); Voltage: 186V (LCS), 200V (316L); WFS: 6.5 m/min; WS: 800 mm/min	The application of heat treatment in WAAM bimetal production balances intermetallic phase formation, leading to improvements in both strength and ductility.	[94]
	LCS (ER70S-6) /316L	GMAW-WAAM (CMT)	Wire diameter: 1.2 mm, Current: 143A (LCS), 214A (316L); Voltage: 21.1V (LCS), 13.2V (316L); WFS: 7.5 m/min (LCS), 5.0 m/min (316L); WS: 10 mm/s.	Hardness: 370 HV UTS: 592 ± 10.7 MPa %el.: 19.8 ± 4.9	[113]
	LCS (ER70S-6)/308LSi	GMAW-WAAM	Wire diameter: 1.2 mm, Current: 105-120 A (LCS), 100–125 A (308LSi); Voltage: 17–19 V (LCS), 18–20 V (308LSi); WFS: 2 m/min (LCS), 3 m/min (308LSi); WS: 150 mm/min	While no intermetallic phase was observed at the interface, diffusion of Cr and Ni elements was observed. UTS: 740.76 MPa, %el.: 21.13	[95]
	LCS (ER70S-6)/304	GMAW-WAAM	Wire diameter: 1.2 mm, Current: 100A (LCS), 143A (304); WS: 5 mm/min	A diffusion region approximately 30 µm thick was found in the interface layer. UTS: 905,9 - 999,8 MPa	[34]
	316L/S214	GMAW-WAAM (CMT)	Wire diameter: 1.2 mm, Current: 80-160A; Voltage: 12.8-20.0V; WFS: 4.0-5.8 m/min^{-1}; WS: 4 mm/s^{-1}	In the interfacial region, Fe-based solid solutions and intermetallic phases such as $AlCrFe_2$, $AlNi_3$, and Al_4Cu_9 were identified. UTS: 340.5 (S214/316), 296,25 (316L/S214)	[104]
Stainless St. / Stainless St.	304L/308L	GMAW-WAAM (CMT)	Wire diameter: 1.2 mm, Current: 147A (Pulse), 200A (Spray); Voltage: 20.3V (Pulse), 23.1V (Spray); WS: 6 mm/sec (Pulse), 9.3 mm/sec. (Spray)	The tensile strength increased in pulse-mode fabricated structures due to the refinement of dendritic structures and the increase in nuclei density. Hardness: 247HV (pulse), UTS: 636 ± 12 MPa (pulse)	[97]
	316L/309	GMAW-WAAM	Current: 110A (316L), 112A (309); Voltage: 18-19V; WFS: 2.3 m/min; WS: 300 mm/min (316L), 296 mm/min (309)	Fe_2O_3, Fe_3O_4, and CrO_2 oxide phases were observed on post-wear surfaces, along with deformation-induced α-martensite formation. Hardness: 240±1,65 HV	[99]
	SS 316L/SS 308L	GMAW-WAAM	Wire diameter: 1.2 mm, Current: 150A; Voltage: 19.5 V; WFS: 5.5 m/sec.; WS: 30 mm/sec.	The interface exhibits a dendritic structure that enhances the strength of the bimetal. UTS: 605,1 ± 5 MPa	[114]
	316L/430	GMAW-WAAM (CMT)	Wire diameter: 1.2 mm, Current: 85-160 A; Voltage: 17.0-21.0 V; WFS: 2.6-5.6 m/min; WS: 0.2-0.4 mm/min^{-1}	With increasing heat input, transformations in the microstructure lead to martensitic formation at the grain boundaries, resulting in elevated high-temperature brittleness. Hardness: 184- 197 HV (316L), 168-176 HV (430), UTS: 220,3 MPa (316L/430), 265,8 MPa (430/316L)	[98]

Stainless steel–based dissimilar alloy systems	316L/Cu	GMAW-WAAM (CMT)	Wire diameter: 1.2 mm, Current: 120A (316L), 130A (Cu); Voltage: 13.6V; WFS: 3.2 m/min; WS: 35 cm/mm	A transition region with an approximate thickness of 6 mm was observed. UTS: 641,33 MPa - 427,33 MPa %el.: 19,78 - %21,80	[101]
	304L/AA2319 (CuNi interlayer)	GMAW-WAAM	Wire diameter: 1.2 mm, Current: 120A (304L-CuNi), 100A (AA2319); WS: 50 cm/min (304L), 60 cm/min (CuNi), 70 cm/min (AA2319)	It was observed that the CuNi interlayer served as an effective diffusion barrier between the 304L and AA2319 layers. Hardness: 242,25 HV (SS304L-CuNi), 517,75 HV (AA2319-CuNi)	[107]
	316L/NiTi	GMAW-WAAM	Wire diameter: 1.2 mm, Voltage: 16.5V; WFS: 5.5 m/min (316L), 5 m/min (NiTi)	Brittle intermetallic compounds, including $TiCr_2$, FeNi, NiTi, $TiNi_3$, and Ti_2Ni, were observed at the NiTi–SS joint interface.	[84]
	316L-Ti	GMAW-WAAM (CMT)	Wire diameter: 1.2 mm, Current: 125 A (316L), 135 A (Ti): Voltage: 13.5 V (316L), 13.8 V (Ti); WFS: 3100 mm/min; WS: 350 mm/min	There are obvious cracks and delamination at the bimetallic interface. Hardness: 967±12 HV	[115]
Steel-cast iron)/ Ni alloys	Grade 91/Monel 400	GMAW-WAAM	Wire diameter: 1.2 mm, Current: 215A (Grade91), 195A (Monel400); Voltage: 22.1V (Grade91), 19.05V (Monel400); WS: 293 mm/min (Grade91), 300 mm/min (Monel400)	It has been observed that Grade 91 steel contains lath martensite and $M_{23}C_6$ carbide precipitates, which increase its strength, while Monel 400 maintains its ductility due to its homogeneous FCC structure.	[102]
	EN-GJS-500-7 cast iron/ Ni- 45 %Fe	GMAW-WAAM (CMT)	Wire diameter: 1.2 mm, Current: 220A Voltage: 20.1V; WFS: 7 m/min; WS: 1000 mm/min	Some cracks and pores have been formed within the interface. UTS: 494-536 MPa, %el.:20.2-17.4	[116]
Other bimetallic systems	Ti6Al4V/NbZr1	GMAW-WAAM	Wire diameter: 0.95 mm, Current: 180-220A; WFS: 1500 mm/min; WS: 200 mm/min	In the interfacial region, island and dendritic zones containing (βTi, Nb) and ($\alpha + \beta$Ti, Nb) solid solutions were observed. Hardness: 99,9- 339 HV UTS: 543,5 MPa, 393 MPa, 367,5 MPa	[108]
	ER80S-G/ MF6 55GP	GMAW-WAAM (CMT)	Wire diameter: 1.2 mm, Current: 82A; Voltage: 12.6V; WFS: 5 m/min^{-1}; WS: 5 mm/s^{-1}	In the interface region, no pores or cracks were found, and a strong metallurgical bond was observed. UTS: 447.79±24.32 MPa	[103]
	S275/IN718	GMAW-WAAM (CMT)	Wire diameter: 1.2 mm, Current: 140-210A; Voltage: 15-16V; WFS: 6-10 m/min; WS: 0.7-1 m/min	The as-built bimetal structure exhibited Laves phase chains along with significant micro segregation.	[105]
	X90/SG2	GMAW-WAAM	Wire diameter: 1.0 mm, Current: 150A; WFS: 7.2 mm/s; WS: 10 mm/s	The diffusion of Ni and Cr between the two steels was detected. YS: 490 MPa, UTS: 600 MPa, %el.:23	[106]

	NiTi/Cu	GMAW-WAAM	Wire diameter: 1.2 mm, Voltage: 16.5 V (Cu), 15 V (NiTi); WFS: 5 m/min	Regions enriched in Cu displayed intensive transformations, highlighting the crucial role of chemical composition in determining the material's behavior.	[117]
	ER50-6/ HS211	GMAW-WAAM	Wire diameter: 1.2 mm, Current: 200A (ER50-6 and interlayer), 230A (HS211); Voltage: 22 V (ER50-6 and interlayer), 25 V (HS211); Speed: 0.3 m/min^{-1}	A melting unmixed zone (UZ) was formed at the interface. UTS: 345,2 MPa	[118]
WS: Welding speed; WFS: Wire feed speed, %el: %elongation; UTS: ultimate tensile strength; YS: yield strength					

3. General remarks and prospects

3.1. Advantages and shortcomings

Bimetal materials have recently gained significant attention owing to their mechanical and physical properties. The WAAM process is advantageous for the production of many different components owing to its high deposition rate and low capital and raw material costs. However, the production of bimetal materials using WAAM is a newly developed research topic. Therefore, there are many advantages and challenges related to both the process and the material when using the WAAM method for bimetal production.

The attainment of high deposition rates in the GMAW-WAAM process offers substantial reductions in production time for large-scale components [54]. Different bimetallic alloys can be produced, and tailored properties can be designed through sequential or stepwise changes in the wire feedstock [119]. Moreover, the use of wire feedstock offers significant advantages over other methods in terms of cost and material waste. GMAW-WAAM enables the fabrication of not only simple geometries but also complex bimetallic structures. Squires et al. [120] successfully demonstrated the production of radial bimetallic components. However, despite these advantages, repeated thermal cycling in WAAM processes can lead to residual stresses and distortions in the layers [121]. Additionally, differences in the thermal expansion coefficients of different wire alloys can cause stress concentrations at bimetallic interfaces. Intermetallic and brittle phase formation also negatively affects the mechanical strength and ductility of bimetallic materials. Therefore, changes in the wire feedstock, parameter control, and geometry optimization must be carefully adjusted to eliminate cracks, pores, residual stresses, and brittle phase formation [54]. Various strategies have been proposed to overcome these challenges. The selection of compatible alloys is crucial for the interface quality in bimetallic production. Optimizing the dwell time and interlayer temperature can effectively reduce residual stresses. Buffer layers in transition regions can prevent the formation of intermetallic phases. Post-processing heat treatments and thermal management techniques are also effective in ensuring microstructural homogeneity and mitigating residual stress.

3.2. Prospects

Nowadays, numerous studies are being conducted on bimetallic production using WAAM. There are opportunities for improvement to address the challenges and limitations of the process. Future research directions include:

1) Different GMAW wires can be developed to expand the diversity of bimetallic production using GMAW-WAAM. These wires can be used to fabricate various bimetallic structures.

2) Intermetallic phases formed in interface regions can be balanced by developing interlayer applications.

3) There are gaps in the literature for many different material combinations. Bimetallic studies on materials such as copper, titanium, and magnesium are still in their early stages. The use of heating and cooling systems can provide thermal cycle control, minimizing residual stress.

4) Hybrid production processes using artificial intelligence tools and robotic automation can be used to optimize the results and potential defects in WAAM bimetal production.

4. Conclusions

This study provides a comprehensive overview of recent advancements in bimetallic structures fabricated using the GMAW-WAAM method. The microstructural characteristics, interface morphology, mechanical properties, and the advantages and challenges of the fabricated bimetallic structures were examined. Studies show that bimetals with strong interface bonds and advanced mechanical properties can be produced by correctly selecting process parameters and material combinations.

1) The GMAW-WAAM method is a promising technique for producing bimetals with various material combinations (stainless steel, copper, nickel, and low-carbon steel). In particular, 316L, IN625, and LCS wires have been common research subjects.

2) It has been observed that, in steel/steel and steel/nickel combinations, the formation of intermetallic phases can be effectively suppressed through appropriate heat input and deposition strategies, thereby enabling the achievement of a sound metallurgical bond.

3) In stainless steel-LCS bimetallic systems, the interfacial characteristics have been reported to be primarily controlled by phase transformations associated with the diffusion of C, Cr, and Ni. The diffusion of carbon toward the stainless steel side leads to martensitic transformations and an increase in hardness at the interface. This indicates that diffusion-induced phase formations are critical to the mechanical properties of the interface.

4) In aluminum-steel, copper-steel, and titanium-based bimetallic systems, the interface exhibits more complex behavior due to limited mutual solubility and mismatches in the coefficient of thermal expansion (CTE). Intermetallic phase formation can be suppressed by reducing the heat input, bidirectional deposition strategies, or by the use of interlayer materials.

5) Chemical incompatibility results in the formation of brittle intermetallic phases and interfacial cracking. Therefore, material selection is a critical parameter in the WAAM-based fabrication of bimetallic structures.

6) Process parameters such as heat input, wire feed speed, and travel speed directly affect the interfacial microstructure and mechanical properties.

7) CMT-based GMAW-WAAM applications provide more balanced mechanical properties due to the lower heat input.

8) Most studies have primarily focused on tensile strength as a mechanical testing method. Performance criteria such as fatigue, creep, corrosion, and impact behaviors are not yet sufficiently understood.

9) Despite the advantages of bimetallic production using GMAW-WAAM, several limitations remain. The formation of intermetallic and brittle phases, porosity, residual stresses, and cracks are among the critical defects. These defects can be overcome by producing new wire materials, optimizing process parameters, and using heat treatments.

The key contribution of this review is the critical of interfacial mechanisms, process-structure-property relationships, and material compatibility considerations in GMAW-WAAM fabricated bimetallic systems, which have previously been reported in a fragmented manner across the literature. For future studies, transition regions and interlayer designs, process and thermal control strategies for interfacial microstructures, hybrid manufacturing approaches integrated into the WAAM process, and optimization studies supported by experimental data are recommended.

Acknowledgements

The authors are grateful for the financial support of Marmara University Scientific Research Fund (BAPKO), Project number: ADF-2023-10864.

Data availability

The datasets generated during and/or analyzed during the current study are available from the corresponding author on reasonable request.

Author contributions

Melike Korganci: conceptualization, data curation, formal analysis, investigation, resources, software, writing - original draft preparation. Nurefşan Kuvvet: conceptualization, data curation, formal analysis, investigation, methodology, software, writing-original draft preparation. Yahya Bozkurt: conceptualization, data curation, methodology, project administration, resources, supervision, validation, visualization, writing-review and editing. Sezgin Ersoy: investigation, methodology, resources, validation, visualization, writing-review and editing.

Conflict of interest

Prof. Sezgin Ersoy is an editorial board member for Journal of Measurements in Engineering and was not involved in the editorial review and/or the decision to publish this article.

References

[1] "Standard terminology for additive manufacturing technologies," ASTM International, West Conshohocken, PA, ASTM F2792-12a, Feb. 2026, https://doi.org/10.1520/f2792-12a

[2] W. E. Frazier, "Metal additive manufacturing: a review," *Journal of Materials Engineering and Performance*, Vol. 23, No. 6, pp. 1917–1928, Apr. 2014, https://doi.org/10.1007/s11665-014-0958-z

[3] A. Alfaify, M. Saleh, F. M. Abdullah, and A. M. Al-Ahmari, "Design for additive manufacturing: a systematic review," *Sustainability*, Vol. 12, No. 19, p. 7936, Sep. 2020, https://doi.org/10.3390/su12197936

[4] B. Baufeld, O. Biest, and R. Gault, "Additive manufacturing of Ti-6Al-4V components by shaped metal deposition: microstructure and mechanical properties," *Materials and Design*, Vol. 31, pp. S106–S111, Jun. 2010, https://doi.org/10.1016/j.matdes.2009.11.032

[5] U. M. Dilberoglu, B. Gharehpapagh, U. Yaman, and M. Dolen, "The role of additive manufacturing in the era of Industry 4.0," *Procedia Manufacturing*, Vol. 11, pp. 545–554, Jan. 2017, https://doi.org/10.1016/j.promfg.2017.07.148

[6] C.-F. Bănică, A. Sover, and D.-C. Anghel, "Printing the future layer by layer: a comprehensive exploration of additive manufacturing in the era of Industry 4.0," *Applied Sciences*, Vol. 14, No. 21, p. 9919, Oct. 2024, https://doi.org/10.3390/app14219919

[7] W. Gao et al., "The status, challenges, and future of additive manufacturing in engineering," *Computer-Aided Design*, Vol. 69, pp. 65–89, Dec. 2015, https://doi.org/10.1016/j.cad.2015.04.001

[8] T. A. Rodrigues, V. Duarte, R. M. Miranda, T. G. Santos, and J. P. Oliveira, "Current status and perspectives on wire and arc additive manufacturing (WAAM)," *Materials*, Vol. 12, No. 7, p. 1121, Apr. 2019, https://doi.org/10.3390/ma12071121

[9] E. Karayel and Y. Bozkurt, "Additive manufacturing method and different welding applications," *Journal of Materials Research and Technology*, Vol. 9, No. 5, pp. 11424–11438, Sep. 2020, https://doi.org/10.1016/j.jmrt.2020.08.039

[10] J. Xiong, Y. Lei, H. Chen, and G. Zhang, "Fabrication of inclined thin-walled parts in multi-layer single-pass GMAW-based additive manufacturing with flat position deposition," *Journal of Materials Processing Technology*, Vol. 240, pp. 397–403, Feb. 2017, https://doi.org/10.1016/j.jmatprotec.2016.10.019

[11] N. Guo and M. C. Leu, "Additive manufacturing: technology, applications and research needs," *Frontiers of Mechanical Engineering*, Vol. 8, No. 3, pp. 215–243, May 2013, https://doi.org/10.1007/s11465-013-0248-8

[12] J. Z. Li, M. R. Alkahari, N. A. B. Rosli, R. Hasan, M. N. Sudin, and F. R. Ramli, "Review of wire arc additive manufacturing for 3D metal printing," *International Journal of Automation Technology*, Vol. 13, No. 3, pp. 346–353, May 2019, https://doi.org/10.20965/ijat.2019.p0346

[13] M. K. Thompson et al., "Design for additive manufacturing: trends, opportunities, considerations, and constraints," *CIRP Annals*, Vol. 65, No. 2, pp. 737–760, Jan. 2016, https://doi.org/10.1016/j.cirp.2016.05.004

[14] T. D. Ngo, A. Kashani, G. Imbalzano, K. T. Q. Nguyen, and D. Hui, "Additive manufacturing (3D printing): A review of materials, methods, applications and challenges," *Composites Part B: Engineering*, Vol. 143, pp. 172–196, Jun. 2018, https://doi.org/10.1016/j.compositesb.2018.02.012

[15] M. Korgancı and Y. Bozkurt, "Recent developments in additive friction stir deposition (AFSD)," *Journal of Materials Research and Technology*, Vol. 30, pp. 4572–4583, May 2024, https://doi.org/10.1016/j.jmrt.2024.04.179

[16] K. V. Wong and A. Hernandez, "A review of additive manufacturing," *ISRN Mechanical Engineering*, Vol. 2012, pp. 1–10, Aug. 2012, https://doi.org/10.5402/2012/208760

[17] S. Ford and M. Despeisse, "Additive manufacturing and sustainability: an exploratory study of the advantages and challenges," *Journal of Cleaner Production*, Vol. 137, pp. 1573–1587, Nov. 2016, https://doi.org/10.1016/j.jclepro.2016.04.150

[18] N. Labonnote, A. Rønnquist, B. Manum, and P. Rüther, "Additive construction: state-of-the-art, challenges and opportunities," *Automation in Construction*, Vol. 72, pp. 347–366, Dec. 2016, https://doi.org/10.1016/j.autcon.2016.08.026

[19] Y. Bozkurt, A. Avşar, M. Korgancı, and G. Çam, "A comprehensive review on friction stir additive manufacturing of various structural alloys for aerospace applications," *Progress in Additive Manufacturing*, Vol. 10, No. 10, pp. 7365–7390, May 2025, https://doi.org/10.1007/s40964-025-01160-y

[20] B. Blakey-Milner et al., "Metal additive manufacturing in aerospace: a review," *Materials and Design*, Vol. 209, p. 110008, Nov. 2021, https://doi.org/10.1016/j.matdes.2021.110008

[21] S. Mohd Yusuf, S. Cutler, and N. Gao, "Review: the impact of metal additive manufacturing on the aerospace industry," *Metals*, Vol. 9, No. 12, p. 1286, Nov. 2019, https://doi.org/10.3390/met9121286

[22] M. Kalender, S. E. Kilic, S. Ersoy, Y. Bozkurt, and S. Salman, "Additive manufacturing and 3D printer technology in aerospace industry," in *9th International Conference on Recent Advances in Space Technologies (RAST)*, pp. 689–694, Jun. 2019, https://doi.org/10.1109/rast.2019.8767881

[23] B. O. Omiyale, T. O. Olugbade, T. E. Abioye, and P. K. Farayibi, "Wire arc additive manufacturing of aluminium alloys for aerospace and automotive applications: a review," *Materials Science and Technology*, Vol. 38, No. 7, pp. 391–408, May 2022, https://doi.org/10.1080/02670836.2022.2045549

[24] F. Lambiase, P. B. Yanala, and A. Paoletti, "Thermal, microstructural, and mechanical characterization of early-stage deposition in wire arc additive manufacturing," *The International Journal of Advanced Manufacturing Technology*, Vol. 138, No. 3-4, pp. 953–970, Apr. 2025, https://doi.org/10.1007/s00170-025-15561-4

[25] D. Jafari, T. H. J. Vaneker, and I. Gibson, "Wire and arc additive manufacturing: opportunities and challenges to control the quality and accuracy of manufactured parts," *Materials and Design*, Vol. 202, p. 109471, Apr. 2021, https://doi.org/10.1016/j.matdes.2021.109471

[26] F. Wang, S. Williams, and M. Rush, "Morphology investigation on direct current pulsed gas tungsten arc welded additive layer manufactured Ti6Al4V alloy," *The International Journal of Advanced Manufacturing Technology*, Vol. 57, No. 5-8, pp. 597–603, Apr. 2011, https://doi.org/10.1007/s00170-011-3299-1

[27] D. Ding, Z. Pan, S. van Duin, H. Li, and C. Shen, "Fabricating superior NiAl bronze components through wire arc additive manufacturing," *Materials*, Vol. 9, No. 8, p. 652, Aug. 2016, https://doi.org/10.3390/ma9080652

[28] D. Ding, Z. Pan, D. Cuiuri, and H. Li, "A multi-bead overlapping model for robotic wire and arc additive manufacturing (WAAM)," *Robotics and Computer-Integrated Manufacturing*, Vol. 31, pp. 101–110, Feb. 2015, https://doi.org/10.1016/j.rcim.2014.08.008

[29] M. Chaturvedi, E. Scutelnicu, C. C. Rusu, L. R. Mistodie, D. Mihailescu, and A. V. Subbiah, "Wire arc additive manufacturing: review on recent findings and challenges in industrial applications and

materials characterization," *Metals*, Vol. 11, No. 6, p. 939, Jun. 2021, https://doi.org/10.3390/met11060939

[30] M. D. Barath Kumar and M. Manikandan, "Assessment of process, parameters, residual stress mitigation, post treatments and finite element analysis simulations of wire arc additive manufacturing technique," *Metals and Materials International*, Vol. 28, No. 1, pp. 54–111, Aug. 2021, https://doi.org/10.1007/s12540-021-01015-5

[31] G. Sharma, S. Rathore, H. Kumar, and K. K. Yadav, "Wear properties of wire and arc additive manufacturing components: a review on recent developments on processes, materials and parameters," *Library Progress International*, Vol. 44, No. 3, pp. 18374–18394, 2024.

[32] K. S. Derekar, "A review of wire arc additive manufacturing and advances in wire arc additive manufacturing of aluminium," *Materials Science and Technology*, Vol. 34, No. 8, pp. 895–916, May 2018, https://doi.org/10.1080/02670836.2018.1455012

[33] D. E. Akpınar, S. Dilibal, and U. Gürol, "Experimental investigation on WAAM-based functional hard-facing bimetallic part," *Journal of Mining and Metallurgy, Section B: Metallurgy*, Vol. 60, No. 2, pp. 283–293, Jan. 2024, https://doi.org/10.2298/jmmb240505020a

[34] Y. Chen et al., "Enhanced strength-ductility synergy of bimetallic laminated steel structure of 304 stainless steel and low-carbon steel fabricated by wire and arc additive manufacturing," *Materials Science and Engineering: A*, Vol. 856, p. 143984, Oct. 2022, https://doi.org/10.1016/j.msea.2022.143984

[35] J. Xiong and G. Zhang, "Adaptive control of deposited height in GMAW-based layer additive manufacturing," *Journal of Materials Processing Technology*, Vol. 214, No. 4, pp. 962–968, Apr. 2014, https://doi.org/10.1016/j.jmatprotec.2013.11.014

[36] L. Zhang et al., "Characterization of GMAW (Gas Metal Arc Welding) penetration using ultrasonics," *Materials*, Vol. 13, No. 10, p. 2307, May 2020, https://doi.org/10.3390/ma13102307

[37] A. Shah, R. Aliyev, H. Zeidler, and S. Krinke, "A review of the recent developments and challenges in wire arc additive manufacturing (WAAM) process," *Journal of Manufacturing and Materials Processing*, Vol. 7, No. 3, p. 97, May 2023, https://doi.org/10.3390/jmmp7030097

[38] A. Vafadar, F. Guzzomi, A. Rassau, and K. Hayward, "Advances in metal additive manufacturing: a review of common processes, industrial applications, and current challenges," *Applied Sciences*, Vol. 11, No. 3, p. 1213, Jan. 2021, https://doi.org/10.3390/app11031213

[39] F. Martina, J. Mehnen, S. W. Williams, P. Colegrove, and F. Wang, "Investigation of the benefits of plasma deposition for the additive layer manufacture of Ti-6Al-4V," *Journal of Materials Processing Technology*, Vol. 212, No. 6, pp. 1377–1386, Jun. 2012, https://doi.org/10.1016/j.jmatprotec.2012.02.002

[40] K. Treutler and V. Wesling, "The current state of research of wire arc additive manufacturing (WAAM): a review," *Applied Sciences*, Vol. 11, No. 18, p. 8619, Sep. 2021, https://doi.org/10.3390/app11188619

[41] C. Xia et al., "A review on wire arc additive manufacturing: monitoring, control and a framework of automated system," *Journal of Manufacturing Systems*, Vol. 57, pp. 31–45, Oct. 2020, https://doi.org/10.1016/j.jmsy.2020.08.008

[42] P. Block, J. Knippers, N. J. Mitra, and W. Wang, *Advances in Architectural Geometry 2014*. Cham: Springer International Publishing, 2015, https://doi.org/10.1007/978-3-319-11418-7

[43] C. R. Cunningham, J. M. Flynn, A. Shokrani, V. Dhokia, and S. T. Newman, "Invited review article: Strategies and processes for high quality wire arc additive manufacturing," *Additive Manufacturing*, Vol. 22, pp. 672–686, Aug. 2018, https://doi.org/10.1016/j.addma.2018.06.020

[44] G. C. Anzalone, C. Zhang, B. Wijnen, P. G. Sanders, and J. M. Pearce, "A low-cost open-source metal 3-D printer," *IEEE Access*, Vol. 1, pp. 803–810, Jan. 2013, https://doi.org/10.1109/access.2013.2293018

[45] B. Wu et al., "A review of the wire arc additive manufacturing of metals: properties, defects and quality improvement," *Journal of Manufacturing Processes*, Vol. 35, pp. 127–139, Oct. 2018, https://doi.org/10.1016/j.jmapro.2018.08.001

[46] T. Le, M. C. Bui, T. D. Nguyen, A. Nguyen, and C. Nguyen, "On the connection of the heat input to the forming quality in wire-and-arc additive manufacturing of stainless steels," *Vacuum*, Vol. 209, p. 111807, Mar. 2023, https://doi.org/10.1016/j.vacuum.2023.111807

[47] M. Srivastava, S. Rathee, A. Tiwari, and M. Dongre, "Wire arc additive manufacturing of metals: A review on processes, materials and their behaviour," *Materials Chemistry and Physics*, Vol. 294, p. 126988, Jan. 2023, https://doi.org/10.1016/j.matchemphys.2022.126988

[48] L. Yan, Y. Chen, and F. Liou, "Additive manufacturing of functionally graded metallic materials using laser metal deposition," *Additive Manufacturing*, Vol. 31, p. 100901, Jan. 2020, https://doi.org/10.1016/j.addma.2019.100901

[49] K. Sanjeeviprakash, A. R. Kannan, and N. S. Shanmugam, "Additive manufacturing of metal-based functionally graded materials: overview, recent advancements and challenges," *Journal of the Brazilian Society of Mechanical Sciences and Engineering*, Vol. 45, No. 5, p. 241, Apr. 2023, https://doi.org/10.1007/s40430-023-04174-1

[50] V. Dhinakaran, J. Ajith, A. Fathima Yasin Fahmidha, T. Jagadeesha, T. Sathish, and B. Stalin, "Wire Arc Additive Manufacturing (WAAM) process of nickel based superalloys – A review," *Materials Today: Proceedings*, Vol. 21, pp. 920–925, Jan. 2020, https://doi.org/10.1016/j.matpr.2019.08.159

[51] O. Yilmaz and A. A. Ugla, "Shaped metal deposition technique in additive manufacturing: a review," *Proceedings of the Institution of Mechanical Engineers, Part B: Journal of Engineering Manufacture*, Vol. 230, No. 10, pp. 1781–1798, Aug. 2016, https://doi.org/10.1177/0954405416640181

[52] B. Dutta and F. H. S. Froes, "The additive manufacturing (AM) of titanium alloys," *Metal Powder Report*, Vol. 72, No. 2, pp. 96–106, Mar. 2017, https://doi.org/10.1016/j.mprp.2016.12.062

[53] H. P. Tang, M. Qian, N. Liu, X. Z. Zhang, G. Y. Yang, and J. Wang, "Effect of powder reuse times on additive manufacturing of Ti-6Al-4V by selective electron beam melting," *JOM*, Vol. 67, No. 3, pp. 555–563, Feb. 2015, https://doi.org/10.1007/s11837-015-1300-4

[54] S. Jadhav et al., "Recent progress and scientific challenges in wire-arc additive manufacturing of metallic multi-material structures," *Journal of Manufacturing and Materials Processing*, Vol. 9, No. 8, p. 284, Aug. 2025, https://doi.org/10.3390/jmmp9080284

[55] D. Ding, Z. Pan, D. Cuiuri, and H. Li, "Wire-feed additive manufacturing of metal components: technologies, developments and future interests," *The International Journal of Advanced Manufacturing Technology*, Vol. 81, No. 1-4, pp. 465–481, May 2015, https://doi.org/10.1007/s00170-015-7077-3

[56] B. A. Szost et al., "A comparative study of additive manufacturing techniques: residual stress and microstructural analysis of CLAD and WAAM printed Ti-6Al-4V components," *Materials and Design*, Vol. 89, pp. 559–567, Jan. 2016, https://doi.org/10.1016/j.matdes.2015.09.115

[57] Y. Bozkurt, H. Gülsoy, and E. Karayel, "The use of additive manufacturing technologies in the production of medical equipment," *El-Cezeri Journal of Science and Engineering*, Vol. 8, No. 2, pp. 962–980, May 2021, https://doi.org/10.31202/ecjse.902023

[58] S. W. Williams, F. Martina, A. C. Addison, J. Ding, G. Pardal, and P. Colegrove, "Wire + arc additive manufacturing," *Materials Science and Technology*, Vol. 32, No. 7, pp. 641–647, May 2016, https://doi.org/10.1179/1743284715y.0000000073

[59] F. Martina, J. Ding, S. Williams, A. Caballero, G. Pardal, and L. Quintino, "Tandem metal inert gas process for high productivity wire arc additive manufacturing in stainless steel," *Additive Manufacturing*, Vol. 25, pp. 545–550, Jan. 2019, https://doi.org/10.1016/j.addma.2018.11.022

[60] W. Zhao, Y. Wei, X. Zhang, J. Chen, and W. Ou, "Comparative investigation of wire arc additive manufacturing of Al-5%Mg alloy with and without external alternating magnetic field," *The International Journal of Advanced Manufacturing Technology*, Vol. 119, No. 3-4, pp. 2571–2587, Jan. 2022, https://doi.org/10.1007/s00170-021-08466-5

[61] D. Yang et al., "Investigation of spatters in cold metal transfer + pulse-based wire and arc additive manufacturing of high nitrogen austenitic stainless steel," *Journal of Materials Engineering and Performance*, Vol. 30, No. 9, pp. 6881–6894, Jul. 2021, https://doi.org/10.1007/s11665-021-06048-w

[62] S. H. Lee, "CMT-based wire arc additive manufacturing using 316L stainless steel: effect of heat accumulation on the multi-layer deposits," *Metals*, Vol. 10, No. 2, p. 278, Feb. 2020, https://doi.org/10.3390/met10020278

[63] Y. Liu, B. Li, W. Zhang, Z. Liu, and M. Jiang, "Interfacial behavior of copper/steel bimetallic composites fabricated by CMT-WAMM," *Coatings*, Vol. 14, No. 7, p. 803, Jun. 2024, https://doi.org/10.3390/coatings14070803

[64] Y. Ali, P. Henckell, J. Hildebrand, J. Reimann, J. P. Bergmann, and S. Barnikol-Oettler, "Wire arc additive manufacturing of hot work tool steel with CMT process," *Journal of Materials Processing Technology*, Vol. 269, pp. 109–116, Jul. 2019, https://doi.org/10.1016/j.jmatprotec.2019.01.034

[65] P. N. Bellamkonda, M. Dwivedy, and R. Addanki, "Cold metal transfer technology – A review of recent research developments," *Results in Engineering*, Vol. 23, p. 102423, Sep. 2024, https://doi.org/10.1016/j.rineng.2024.102423

[66] A. Schierl, "The CMT-process-a revolution in welding technology," *Weld World*, Vol. 49, No. 9, pp. 1–10, 2005.

[67] S. Sirohi et al., "Microstructure and mechanical properties of combined GTAW and SMAW dissimilar welded joints between Inconel 718 and 304L austenitic stainless steel," *Metals*, Vol. 13, No. 1, p. 14, Dec. 2022, https://doi.org/10.3390/met13010014

[68] C. Wei, Z. Zhang, D. Cheng, Z. Sun, M. Zhu, and L. Li, "An overview of laser-based multiple metallic material additive manufacturing: from macro – to micro-scales," *International Journal of Extreme Manufacturing*, Vol. 3, No. 1, p. 012003, Jan. 2021, https://doi.org/10.1088/2631-7990/abce04

[69] Y. Cui et al., "Multi-material additive manufacturing of steel/Al alloy by controlling the liquid/solid interface in laser beam powder bed fusion," *Additive Manufacturing*, Vol. 96, p. 104529, Sep. 2024, https://doi.org/10.1016/j.addma.2024.104529

[70] M. Tisza and I. Czinege, "Comparative study of the application of steels and aluminium in lightweight production of automotive parts," *International Journal of Lightweight Materials and Manufacture*, Vol. 1, No. 4, pp. 229–238, Dec. 2018, https://doi.org/10.1016/j.ijlmm.2018.09.001

[71] W. W. Wits and E. Amsterdam, "Graded structures by multi-material mixing in laser powder bed fusion," *CIRP Annals*, Vol. 70, No. 1, pp. 159–162, Jan. 2021, https://doi.org/10.1016/j.cirp.2021.03.005

[72] V. Bhanu, A. Gupta, and C. Pandey, "Role of A-TIG process in joining of martensitic and austenitic steels for ultra-supercritical power plants – a state of the art review," *Nuclear Engineering and Technology*, Vol. 54, No. 8, pp. 2755–2770, Aug. 2022, https://doi.org/10.1016/j.net.2022.03.003

[73] K. Martinsen, S. J. Hu, and B. E. Carlson, "Joining of dissimilar materials," *CIRP Annals*, Vol. 64, No. 2, pp. 679–699, Jan. 2015, https://doi.org/10.1016/j.cirp.2015.05.006

[74] S. O. Rogachev, V. A. Andreev, V. S. Yusupov, S. A. Bondareva, V. M. Khatkevich, and E. V. Nikolaev, "Effect of rotary forging on microstructure evolution and mechanical properties of aluminum alloy/copper bimetallic material," *Metals and Materials International*, Vol. 28, No. 4, pp. 1038–1046, May 2021, https://doi.org/10.1007/s12540-020-00964-7

[75] W. Jiang, F. Guan, G. Li, H. Jiang, J. Zhu, and Z. Fan, "Processing of Al/Cu bimetal via a novel compound casting method," *Materials and Manufacturing Processes*, Vol. 34, No. 9, pp. 1016–1025, Jul. 2019, https://doi.org/10.1080/10426914.2019.1615084

[76] A. Kumar and C. Pandey, "Structural integrity assessment of Inconel 617/P92 steel dissimilar welds for different groove geometry," *Scientific Reports*, Vol. 13, No. 1, p. 92, May 2023, https://doi.org/10.1038/s41598-023-35136-1

[77] A. Garga, S. Kumar, Hirshikesh, and C. Pandey, "Comparative assessment of Ni-based electrodes on the integrity of Inconel 617-AISI 304 H dissimilar welds for advanced ultra-supercritical boilers," *Materials Today Communications*, Vol. 50, p. 114254, Jan. 2026, https://doi.org/10.1016/j.mtcomm.2025.114254

[78] A. Bandyopadhyay, Y. Zhang, and B. Onuike, "Additive manufacturing of bimetallic structures," *Virtual and Physical Prototyping*, Vol. 17, No. 2, pp. 256–294, Apr. 2022, https://doi.org/10.1080/17452759.2022.2040738

[79] S. Yadav, C. P. Paul, A. K. Rai, A. N. Jinoop, and S. K. Dixit, "Effect of interlayer composition on the properties of laser-directed-energy-deposition-based additively manufactured copper-stainless steel wall structures," *Sustainability*, Vol. 16, No. 2, p. 519, Jan. 2024, https://doi.org/10.3390/su16020519

[80] M. M. El-Husseiny, A. A. Baraka, O. Oraby, E. A. El-Danaf, and H. G. Salem, "Fabrication of bimetallic high-strength low-alloy steel/si-bronze functionally graded materials using wire arc additive manufacturing," *Journal of Manufacturing and Materials Processing*, Vol. 7, No. 4, p. 138, Jul. 2023, https://doi.org/10.3390/jmmp7040138

[81] T. A. Rodrigues et al., "Steel-copper functionally graded material produced by twin-wire and arc additive manufacturing (T-WAAM)," *Materials and Design*, Vol. 213, p. 110270, Jan. 2022, https://doi.org/10.1016/j.matdes.2021.110270

[82] A. Dhanola and D. S. Prasad, "A comprehensive review of wire arc additive manufacturing for metallic functionally graded materials," *Engineering Research Express*, Vol. 6, No. 4, p. 042501, Dec. 2024, https://doi.org/10.1088/2631-8695/ad82a4

[83] K. U. Rani et al., "Wire arc additive manufactured mild steel and austenitic stainless steel components: microstructure, mechanical properties and residual stresses," *Materials*, Vol. 15, No. 20, p. 7094, Oct. 2022, https://doi.org/10.3390/ma15207094

[84] S. Singh, A. N. Jinoop, I. A. Palani, C. P. Paul, K. P. Tomar, and K. G. Prashanth, "Microstructure and mechanical properties of NiTi-SS bimetallic structures built using wire arc additive manufacturing," *Materials Letters*, Vol. 303, p. 130499, Nov. 2021, https://doi.org/10.1016/j.matlet.2021.130499

[85] G. Gogulraj and G. Rajamurugan, "Overlapped weld bead analysis on dissimilar duplex stainless steel-2507 and inconel-625 using WAAM-CMT process," *Results in Engineering*, Vol. 28, p. 107290, Dec. 2025, https://doi.org/10.1016/j.rineng.2025.107290

[86] S. Bai and J. Liu, "Additive manufacturing of bimetallic structures," *SN Applied Sciences*, Vol. 2, No. 7, p. 1152, July 2020, https://doi.org/10.1007/s42452-020-2918-6.

[87] M. R. U. Ahsan et al., "Microstructures and mechanical behavior of the bimetallic additively-manufactured structure (BAMS) of austenitic stainless steel and Inconel 625," *Journal of Materials Science and Technology*, Vol. 74, pp. 176–188, May 2021, https://doi.org/10.1016/j.jmst.2020.10.001

[88] S.-W. Yoo, C.-M. Lee, and D.-H. Kim, "Effect of functionally graded material (FGM) interlayer in metal additive manufacturing of inconel-stainless bimetallic structure by laser melting deposition (LMD) and wire arc additive manufacturing (WAAM)," *Materials*, Vol. 16, No. 2, p. 535, Jan. 2023, https://doi.org/10.3390/ma16020535

[89] R. Sasikumar et al., "Wire arc additive manufacturing of functionally graded material with SS 316L and IN625: Microstructural and mechanical perspectives," *CIRP Journal of Manufacturing Science and Technology*, Vol. 38, pp. 230–242, Aug. 2022, https://doi.org/10.1016/j.cirpj.2022.05.005

[90] A. Motwani, A. Kumar, Y. Puri, and N. K. Lautre, "Mechanical characteristics and microstructural investigation of CMT deposited bimetallic SS316LSi-IN625 thin wall for WAAM," *Welding in the World*, Vol. 67, No. 4, pp. 967–980, Nov. 2022, https://doi.org/10.1007/s40194-022-01403-4

[91] W. Zhang, Y. Lei, W. Meng, Q. Ma, X. Yin, and L. Guo, "Effect of deposition sequence on microstructure and properties of 316L and Inconel 625 bimetallic structure by wire arc additive manufacturing," *Journal of Materials Engineering and Performance*, Vol. 30, No. 12, pp. 8972–8983, Aug. 2021, https://doi.org/10.1007/s11665-021-06137-w

[92] L. P. Raut and R. V. Taiwade, "Microstructure and mechanical properties of wire arc additively manufactured bimetallic structure of austenitic stainless steel and low carbon steel," *Journal of Materials Engineering and Performance*, Vol. 31, No. 10, pp. 8531–8541, Apr. 2022, https://doi.org/10.1007/s11665-022-06856-8

[93] F. Marefat, J. de Pauw, A. Kapil, N. Chernovol, P. van Rymenant, and A. Sharma, "Design strategies for bi-metallic additive manufacturing in the context of wire and arc directed energy deposition," *Materials and Design*, Vol. 215, p. 110496, Mar. 2022, https://doi.org/10.1016/j.matdes.2022.110496

[94] M. R. U. Ahsan et al., "Heat-treatment effects on a bimetallic additively-manufactured structure (BAMS) of the low-carbon steel and austenitic-stainless steel," *Additive Manufacturing*, Vol. 32, p. 101036, Mar. 2020, https://doi.org/10.1016/j.addma.2020.101036

[95] Y. Ayan and N. Kahraman, "Fabrication and characterization of functionally graded material (FGM) structure containing two dissimilar steels (ER70S-6 and 308LSi) by wire arc additive manufacturing (WAAM)," *Materials Today Communications*, Vol. 33, p. 104457, Dec. 2022, https://doi.org/10.1016/j.mtcomm.2022.104457

[96] P. Sędek, J. Brózda, L. Wang, and P. J. Withers, "Residual stress relief in MAG welded joints of dissimilar steels," *International Journal of Pressure Vessels and Piping*, Vol. 80, No. 10, pp. 705–713, Oct. 2003, https://doi.org/10.1016/j.ijpvp.2003.08.004

[97] S. B. Ainapurapu, V. A. R. Devulapalli, R. P. Theagarajan, B. K. Chigilipalli, R. K. Kottala, and M. Cheepu, "Microstructure and mechanical properties of the bimetallic wire arc additively manufactured structure (BAMS) of SS304L and SS308L fabricated by hybrid manufacturing process," *Transactions of the Indian Institute of Metals*, Vol. 76, No. 2, pp. 419–426, Aug. 2022, https://doi.org/10.1007/s12666-022-02695-2

[98] X. Wang et al., "Microstructure evolution and mechanical properties of ferrite-austenite stainless steel bimetals fabricated via wire arc additive manufacturing," *Steel Research International*, Vol. 95, No. 3, p. 23004, Dec. 2023, https://doi.org/10.1002/srin.202300494

[99] R. S. Tanwar and S. Jhavar, "Microstructure and tribological characterization of thin wall of bimetallic austenitic steel fabricated through wire arc additive manufacturing (WAAM)," *Applications in Engineering Science*, Vol. 23, p. 100241, Sep. 2025, https://doi.org/10.1016/j.apples.2025.100241

[100] H. Kaur, S. Kumar, D. Malhotra, and T. Nanda, "Corrosion and metallurgical behavior of wire arc additively manufactured functionally graded super duplex stainless steel/Inconel 625," *Journal of Materials Engineering and Performance*, Vol. 33, No. 24, pp. 14011–14028, Nov. 2023, https://doi.org/10.1007/s11665-023-08988-x

[101] B. Tomar and S. Shiva, "Microstructural and mechanical properties examination of SS316L-Cu functionally graded material fabricated by wire arc additive manufacturing," *CIRP Journal of Manufacturing Science and Technology*, Vol. 50, pp. 26–39, Jun. 2024, https://doi.org/10.1016/j.cirpj.2024.02.002

[102] S. Munusamy and J. J., "Effect of build orientation on the microstructure and mechanical properties of wire arc additive manufactured grade 91 steel/Monel 400 bimetallic components," *Vacuum*, Vol. 227, p. 113429, Sep. 2024, https://doi.org/10.1016/j.vacuum.2024.113429

[103] S. Han, Z. Zhang, Z. Liu, H. Zhang, and D. Xue, "Investigation of the microstructure and mechanical performance of bimetal components fabricated using CMT-based wire arc additive manufacturing," *Materials Research Express*, Vol. 7, No. 11, p. 116525, Nov. 2020, https://doi.org/10.1088/2053-1591/abcb4b

[104] W. Meng et al., "Interfacial characteristics and mechanical properties of 316L and S214 bimetals fabricated by wire-arc additive manufacturing," *Advanced Engineering Materials*, Vol. 26, No. 2, p. 23015, Dec. 2023, https://doi.org/10.1002/adem.202301504

[105] N. Hasani et al., "Dislocations mobility in superalloy-steel hybrid components produced using wire arc additive manufacturing," *Materials and Design*, Vol. 220, p. 110899, Aug. 2022, https://doi.org/10.1016/j.matdes.2022.110899

[106] N. Spalek, J. Brunow, M. Braun, and M. Rutner, "WAAM-fabricated laminated metal composites," *Metals*, Vol. 11, No. 12, p. 1948, Dec. 2021, https://doi.org/10.3390/met11121948

[107] G. Manohar, A. Kumar, S. Thapliyal, and R. Mamedipaka, "Investigating the performance of aluminium-steel bimetallic structure fabricated through wire and arc additive manufacturing with interlayer approach," *Structures*, Vol. 72, p. 108304, Feb. 2025, https://doi.org/10.1016/j.istruc.2025.108304

[108] S. Jadhav et al., "Materials characterization of Ti6Al4V to NbZr1 bimetallic structure fabricated by wire arc additive manufacturing," *Materials Today Communications*, Vol. 36, p. 106934, Aug. 2023, https://doi.org/10.1016/j.mtcomm.2023.106934

[109] S. Kesarwani, N. Yuvaraj, and M. S. Niranjan, "Impact of depositional direction and current on microstructure and mechanical properties of the bimetallic wall of ER5356/ER4043 fabricated by cold metal transfer based wire arc additive manufacturing," *CIRP Journal of Manufacturing Science and Technology*, Vol. 53, pp. 17–33, Oct. 2024, https://doi.org/10.1016/j.cirpj.2024.06.013

[110] S. Mohan Kumar et al., "Microstructural features and mechanical integrity of wire arc additive manufactured SS321/Inconel 625 functionally gradient material," *Journal of Materials Engineering and Performance*, Vol. 30, No. 8, pp. 5692–5703, Mar. 2021, https://doi.org/10.1007/s11665-021-05617-3

[111] T. Abe and H. Sasahara, "Dissimilar metal deposition with a stainless steel and nickel-based alloy using wire and arc-based additive manufacturing," *Precision Engineering*, Vol. 45, pp. 387–395, Jul. 2016, https://doi.org/10.1016/j.precisioneng.2016.03.016

[112] A. S. Azar, A. Lekatou, M. F. Sunding, J. S. Graff, N. Tzima, and S. Diplas, "Corrosion performance and degradation mechanism of a bi-metallic aluminum structure processed by wire-arc additive manufacturing," *NPJ Materials Degradation*, Vol. 5, No. 1, p. 26, May 2021, https://doi.org/10.1038/s41529-021-00175-4

[113] J. L. Galán Argumedo, M. Mahmoudiniya, T. E. Reinton, L. A. I. Kestens, M. J. M. Hermans, and V. A. Popovich, "Functional grading of low alloy steel to 316 L by wire arc additive manufacturing – Microstructural and mechanical characterization of bi-metal interface," *Journal of Materials Processing Technology*, Vol. 325, p. 118305, Apr. 2024, https://doi.org/10.1016/j.jmatprotec.2024.118305

[114] A. Thirugnanasambandam, M. K. Subramaniyan, and V. Elumalai, "Fabrication of bimetallic structure (SS 316L/SS 308L) via wire + arc additive manufacturing: a detailed characterization of interface," *Journal of Materials Engineering and Performance*, Vol. 34, No. 15, pp. 16297–16308, Oct. 2024, https://doi.org/10.1007/s11665-024-10298-9

[115] B. Tomar and S. Shiva, "Analysis of AISI 316L-Ti graded deposition fabricated by wire and arc additive manufacturing," *Transactions of the Indian Institute of Metals*, Vol. 77, No. 1, pp. 279–285, Sep. 2023, https://doi.org/10.1007/s12666-023-03101-1

[116] M. Mahmoudiniya, A.-S. Thorr, R. H. Petrov, M. J. M. Hermans, and L. A. I. Kestens, "Wire arc additive manufacturing of Ni Fe alloy/ductile cast iron bimetallic structure; phase transformations, microstructure and crystallographic texture," *Materials Characterization*, Vol. 220, p. 114650, Feb. 2025, https://doi.org/10.1016/j.matchar.2024.114650

[117] S. Singh et al., "NiTi-Cu bimetallic structure fabrication through wire arc additive manufacturing," *Materials*, Vol. 17, No. 5, p. 1006, Feb. 2024, https://doi.org/10.3390/ma17051006

[118] M. Zhang, Y. Zhang, M. Du, S. Zhang, and L. Lei, "Experimental characterization and microstructural evaluation of silicon bronze-alloy steel bimetallic structures by additive manufacturing," *Metallurgical and Materials Transactions A*, Vol. 52, No. 10, pp. 4664–4674, Aug. 2021, https://doi.org/10.1007/s11661-021-06418-y

[119] R. S. Tanwar and S. Jhavar, "Multi-wire additive manufacturing: a comprehensive review on materials, microstructure, methodological advances, and applications," *Results in Engineering*, Vol. 26, p. 104814, Jun. 2025, https://doi.org/10.1016/j.rineng.2025.104814

[120] L. Squires, E. Roberts, and A. Bandyopadhyay, "Radial bimetallic structures via wire arc directed energy deposition-based additive manufacturing," *Nature Communications*, Vol. 14, No. 1, p. 3544, Jun. 2023, https://doi.org/10.1038/s41467-023-39230-w

[121] F. Gurmesa, H. Lemu, Y. Adugna, and M. Harsibo, "Residual stresses in wire arc additive manufacturing products and their measurement techniques: a systematic review," *Applied Mechanics*, Vol. 5, No. 3, pp. 420–449, Jul. 2024, https://doi.org/10.3390/applmech5030025

Melike Korgancı graduated from Marmara University, Department of Metallurgical and Materials Engineering in 2017. She is currently a research assistant and Ph.D. student at Marmara University. Her current research activities include the development of additive manufacturing, welding technologies, materials science, and engineering.

Nurefşan Kuvvet graduated from Marmara University, Department of Metallurgical and Materials Engineering in 2024. She is a research assistant in the Department of Metallurgical and Materials Engineering. She is currently pursuing her M.Sc. degree in the same field. Her research interests include composite materials, welding technologies, and additive manufacturing.

Yahya Bozkurt received his Ph.D. degree from the Metal Education Department of the Technical Education Faculty at Marmara University, Institute of Pure and Applied Sciences. He has been a full Professor in the Metallurgy and Materials Engineering Department since 2018. His research areas include welding technologies, solid-state welding, manufacturing methods, 3D printing technology, and additive manufacturing.

Sezgin Ersoy received his Ph.D. degree in Material Science from Marmara University, Istanbul, Türkiye in 2012. He is currently working at Marmara University. His current research interests include mechatronic, automotive, material science and machine engineering.